Fluid Dynamics Research

The Japan Society of Fluid Mechanics

Group theory and jelly's experiment of Rayleigh-Taylor instability and Rayleigh-Taylor interfacial mixing

To cite this article before publication: Evgeny E Meshkov *et al* 2019 *Fluid Dyn. Res.* in press https://doi.org/10.1088/1873-7005/ab3e83

Group theory and jelly's experiment of Rayleigh-Taylor instability and Rayleigh-Taylor interfacial mixing

Evgeny E. Meshkov (1); Snezhana I. Abarzhi* (2)
Sarov Institute for Physics and Technology, National Nuclear Research University, Russia (1)
The University of Western Australia, Australia (2)
*corresponding author email: snezhana.abarzhi@gmail.com

Rayleigh-Taylor instability develops at the interface between two fluids of different densities accelerated against their density gradients. Intense interfacial fluid mixing ensues with time. Rayleigh-Taylor mixing controls a broad range of processes in fluids, plasmas, materials, at astrophysical and at molecular scales. In this work we focus on the physics of Rayleigh-Taylor mixing, which we have identified through our theoretical and experimental studies. The theory analyzes symmetries and invariants of Rayleigh-Taylor dynamics and finds that Rayleigh-Taylor mixing has strong correlations, weak fluctuations, and is sensitive to deterministic conditions. The experiment unambiguously observes heterogeneity, anisotropy and sensitivity to deterministic conditions of Rayleigh-Taylor mixing in a broad range of setups. The theory and the experiment agree with one another, reveal that Rayleigh-Taylor mixing may exhibit order and suggest new avenue for studies interfacial mixing in nature and technology.

Keywords: interfacial dynamics, Rayleigh-Taylor instability, Rayleigh-Taylor mixing
PACS: 47.20.Ma, 47.20.-k, 52.35.-g, 52.35.Py

1. Introduction

We observe Rayleigh-Taylor instability (RTI) when watching water flowing from an overturned cup [1]. RTI develops when fluids of different densities are accelerated against their density gradients, and/or when the fluid interface moves with an acceleration directed toward the denser fluid and normal to the interface [2]. RTI leads to the growth of the interface perturbations in the acceleration direction. Intense interfacial Rayleigh-Taylor (RT) mixing of the fluids ensues with time [3-5]. RT mixing is heterogeneous, anisotropic, and statistically unsteady process with non-local interactions among the many scales [3-5]. Its properties may depart from those of homogeneous, isotropic, local, and statistically steady turbulence [3,6]. One has to grasp the fundamentals of RT mixing to better understand a broad range of RT-relevant phenomena in nature and technology and to elaborate new methods of studies of non-equilibrium dynamics [3-7].

RTI and RT mixing control a broad range of processes in fluids, plasmas, materials [7]. These processes can be natural and artificial, their characteristic scales can be astrophysical and atomic, and energy densities can be low and high [7]. Examples include inertial confinement and magnetic fusion, formation of accretion disk and explosion of supernova, material transformation under impact and free-space optical communications, dynamics of reactive fluids and fossil fuel extraction [7].

RT flows arising in the vastly different physical regimes exhibit a number of similar features of their evolution [1-5]. RTI starts to develop when the fluid interface and/or the flow fields are slightly perturbed near the state of (unstable) equilibrium [1,2]. The flow develops from an initial stage where the perturbation amplitude grows quickly (exponentially in time) to a nonlinear stage where the growth slows (to a power-law in time) [2,3,8]. The interface is transformed to a composition of large-scale coherent structure of bubbles and spikes (with the light (heavy) fluid penetrating the heavy (light) fluid in bubbles (spikes)), and small-scale shear-driven vortical irregular structures [2,4]. The final stage of RTI is the interfacial mixing, whose dynamics is believed to be self-similar [3-12]. Particularly, in RT mixing driven by a constant acceleration, the flow length scale in the acceleration direction grows quadratic in time [9-11]. RT dynamics is usually three-dimensional (3D) [3-5,8].

An RT flow is a ‘mixture’ of multifaceted properties complementing one another [3-5,8-12]. RT mixing has certain degree of order; and yet, it is a noisy process with strong coupling of all the scales [3,8,9]. RT mixing is believed to be self-similar; and yet, it is sensitive to deterministic and initial conditions [3,9-12]. Accelerated RT mixing is characterized by increasing values of the Reynolds number, velocity scale and energy dissipation rate – whose large values are necessary conditions for turbulence to occur, - and yet, RT flow fields are heterogeneous, even in statistical sense, its dynamics in the acceleration direction differs from that in the normal plane, and its quantities have the mean values varying in time [3-12]. In this work we apply theory and experiment to better understand the physics of RT mixing and the potential impact of this knowledge on future research.

RTI and RT mixing are an extreme challenge to study in their direct manifestations [7]. In experiments, the transient character and sensitivity of large scale dynamics to small scales and the deterministic and initial conditions impose tight requirements on the implementation, control and

diagnostics of RT flows [4,5,12-16,63]. In simulations, the needs to accurately track interfaces and capture dissipative processes demand the use of highly accurate numerical methods and massive computations [9-11]. In theory, the necessity to identify the universal properties of asymptotic solutions, grasp symmetry of RT flows and account for their noisiness the development of new methods of study of non-equilibrium, multi-scale, nonlinear, and non-local dynamics [3,5,8]. A systematic interpretation of RT dynamics from data is a challenge that calls for robust parameters to be precisely diagnosed [3-5,7-16]. Furthermore, for reliable quantification of power-laws describing the statistically unsteady RT mixing, the flow diagnostics demands high accuracy, high precision, high data acquisition rate, and substantial span of resolved scales in space and in time [3-5,7-17].

Despite these challenges, significant success has been recently achieved in our understanding of RT dynamics [3,5,7,12,63]. In fluid experiments, the experimental design and advanced diagnostics have enabled implementations and measurements of RT mixing, including the growth-rate and the fluctuations' statistics [4,12-15]. In high energy density plasmas, certain progress has been achieved in mimicking RT-driven astrophysical phenomena in laboratory [5,16]. In simulations, the Eulerian and Lagrangian methods have provided detailed information on the dynamics and morphology of RT unstable interface and RT mixing [9-11]. Efficient computational methods have been developed to model the effect of turbulence (assuming it may develop) on RT mixing, and to estimate in practice the influence of this hydrodynamic noise on parameters of RT-relevant phenomena [10,18]. In theory, significant success has been reached in the understanding of fundamental properties of RTI and RT mixing [3,5,8]. For outline of the state-of-the-art experiments, theory and simulations and for rigorous physics-based discussion of properties of RTI and RT mixing, the reader is referred to research books and review papers [3-5,7-13].

Here we apply the theory and the experiment to study RT dynamics, with focus on acceleration effect on order and disorder in RT mixing, Table 1 – Table 16, Figure 1 – Figure 15 [3-5,8,12]. The analysis is based on group theory, identifies symmetries and invariants of RT dynamics, and finds that RT mixing has strong correlations and weak fluctuations; it is sensitive to deterministic conditions and may exhibit order [3,5,8,19-26]. The experiment unambiguously observe heterogeneity, anisotropy and sensitivity to deterministic and initial conditions of RT mixing at Reynolds numbers up to ~3.2 million [3,5,12,27-33]. The theory and the experiment agree with one another and suggest that RT mixing may keep order and laminarize, similarly to other classical accelerated flows, such as flows in curved pipes and accelerated boundary layers [34,35]. The other data available indicate that for precise quantification of RT mixing a substantial span of resolved scales is required, to be achieved in the future [3,5,8,12,15,17].

2. Methods

2.1 Theory

2.1.1 Governing equations

RT dynamics of ideal fluids is governed by the conservation of mass, momentum and energy. In the inertial frame of reference the governing equations are

$$\frac{\partial \rho}{\partial t}+\frac{\partial \rho v_i}{\partial x_i}=0, \quad \frac{\partial \rho v_i}{\partial t}+\sum_{j=1}^{3}\frac{\partial \rho v_i v_j}{\partial x_j}+\frac{\partial P}{\partial x_i}=0, \quad \frac{\partial E}{\partial t}+\frac{\partial (E+P)v_i}{\partial x_i}=0 \tag{1a}$$

Here $\{x_1, x_2, x_3\}=\{x, y, z\}$ are spatial coordinates with, t is time, $\{\rho, \mathbf{v}, P, E\}$ are the fields of density ρ, velocity $\mathbf{v}$, pressure P, energy $E=\rho\left(e+\mathbf{v}^2/2\right)$, and e is specific internal energy [36]. In the bulk of the heavy (light) fluid the flow fields are $\{\rho, \mathbf{v}, P, E\}_{h(l)}$.

At the interface, for immiscible fluids the fluxes of mass, normal and tangential components of momentum and energy obey the conditions

$$[\mathbf{v}\cdot\mathbf{n}]=0, \quad [P]=0, \quad [\mathbf{v}\cdot\boldsymbol{\tau}]=arbitrary, \quad [W]=arbitrary \tag{1b}$$

Here $[...]$ denotes the jump of functions at the interface; $\mathbf{n}$ and $\boldsymbol{\tau}$ are the normal and tangential unit vectors of the interface; $W=e+P/\rho$ is specific enthalpy. Boundary conditions Eqs.(1b) are derived from the governing equations Eqs.(1a) in the inertial frame of reference in case of zero mass flux across the moving interface [61,62], in complete consistency with the classical results [36,58,61,62].

The flow has no external sources, and boundary conditions at the outside boundaries are:

$$\mathbf{v}|_{z\to+\infty}=0, \qquad \mathbf{v}|_{z\to-\infty}=0 \tag{1c}$$

Boundary conditions Eqs.(1c) correspond to the laboratory frame of reference, in which the velocity of the inertial frame of reference is zero [36,58,61,62].

Initial conditions close the set of the governing equations and include initial perturbations of the flow fields in the bulk and at the interface [3,8,36]. In the presence of kinematic viscosity ν and other non-ideal effects the governing equations are further modified [36].

The flow can be periodic in the plane (x, y), and is subject to acceleration (gravity) $\mathbf{g}$, $|\mathbf{g}|=g$, $\mathbf{g}=(0,0,-g)$ directed from the heavy to the light fluid along the z -axis, Figure 1. The presence of acceleration modifies the pressure term in Eqs.(1).

Note that mathematical problem Eqs.(1) of RTI and RT mixing requires one to solve a system of nonlinear partial differential equations in four-dimensional space-time, the boundary value problems for a sub-set of nonlinear partial differential equations at a nonlinear freely evolving interface and at outside boundaries, and the ill-posed initial value problem with account for finite-time singularities [3,5,8]. This mathematical problem may be more challenging than the problems of canonical turbulence and Navier-Stokes equation [17,37]. Rigorous theories have solved the governing equations in well-defined approximations; empirical models have described the data with similar sets of adjustable parameters [3,5,8,19-26,38-45].

2.1.2 Outline of theoretical approaches and group theory approach

In the linear regime of RTI, small perturbations of the flow field grow with time, $\sim exp(t/\tau)$, where $\tau \sim \sqrt{\lambda/Ag}$ is time-scale, λ is the initial perturbation wavelength, $A=(\rho_h-\rho_l)/(\rho_h+\rho_l)$ is the Atwood number Figure 1 [1,2,36]. The RTI growth-rate can be influenced by viscosity, surface tension, compressibility, thermal conductivity, magnetic fields and other effects [3,8,38-41]. They usually stabilize small scales with $\lambda<\lambda_c$, where λ_c is a critical wavelength, and set a characteristic length-scale λ_m, $\lambda_m>\lambda_c$, at which the maximum growth-rate is achieved. In case of kinematic viscosity ν, the characteristic length-scale is $\lambda_m \sim (\nu^2/g)^{1/3}$, and a characteristic time-scale is $\tau_m \sim (\nu/g^2)^{1/3}$ [39]. For large (small) wavelengths with $\lambda/\lambda_m \to \infty(0)$, the growth-rate of RTI is small compared to that at λ_m [39]. Group theory can be employed to derive the growth-rate of RTI for initial perturbations with various symmetries Figure 2 [8,23].

As time progresses, the exponential growth of the amplitude of the interface perturbations is superseded by a time-dependent power-law. Weakly-nonlinear RTI in ideal fluids has been studied theoretically and empirically with focus on the effect of initial spectra on RTI growth-rate [3,8,39,41]. The models have found that standard perturbation approaches work well only at early times and for small amplitudes [3,8,39,41]. Furthermore, nonlinear RT dynamics is accompanied by singularities [3,5,8,41]. The singular character of the RTI is exhibited in, e.g., multiplicity of nonlinear regular asymptotic solutions [3,8,19-22,42,43]. Group theory approach has successfully resolved the nonlinear boundary value problem and has identified local and global properties of coherent RT dynamics [3,5,8,19-22,44].

The interactions of RT bubbles may lead to the growth of the wavelength(s) (periods) of the coherent structure and the bubble merge and may trigger a transition to self-similar RT mixing [8,9-12,22,23]. This transition has been investigated by the model [11,45] that has excellently agreed with data. The data on RT mixing have been accurately interpolated by the model [10]. Group theory has been applied to classify patterns' formation and interactions in RT flows and identify possible discrete transitions with increase of the coherent structure wavelength(s) under the influence of modulations, in excellent agreement with experiments [22,23,46].

By assuming that RT mixing is similar to canonical turbulence, several models have substituted the growth-rate of RT mixing in turbulent scaling laws to compute possible turbulence effects [10,18,47]. By being harmonious with the turbulence theory [6,36] and with the models [10,11,18,45,47], and by scrupulously analyzing symmetries and invariants of RT dynamics, group theory [3,5,8,24-26,48] has found properties of RT mixing which have not been identified in other studies. This includes the properties of invariance, correlations and fluctuations and the sensitivity to deterministic conditions [3,25]. Here we focus on group theory approach to better understand the physics of RT dynamics, explain the experiments, and elaborate benchmarks for future research.

Group theory is a powerful tool of theoretical physics and applied mathematics. It is known for its effectiveness in solving a broad class of mathematical problems describing natural processes. In fluid

dynamics, group theory (and, particularly, theory of space discrete groups) is applied to study spatially ordered structures in Rayleigh-Benard convection [59,60].

2.2 Experiment

2.2.1 Outline of experimental challenges

It is easy to overturn a cup of water to observe RTI. It is an extreme challenge to reliably implement RT flows in a laboratory, and to systematically probe and gather precise and accurate data on RT dynamics in experiment [1,2,4,12,13]. On the side of implementation, RT flows are sensitive to initial and boundary conditions at the interface and the outside boundaries, to acceleration history, fluids' properties and experimental bias at large and at small scales [4,12-16]. On the side of diagnostics, many powerful methods have been developed for probing fluid flows [13,17]. They range from measurements of average velocities to the Schlieren and shadowgraph techniques, thermal anemometry, laser Doppler velocimetry, planar laser induced fluorescence and particle image velocimetry [13]. These methods have substantially advanced our knowledge of canonical turbulence [13,17]. Their capabilities in RT flows are somewhat bounded by resolution limitations and the flow sensitivity to the measurement technology [4,12-16].

On the data gathering side, RT flows are characterized by statistically unsteady transports of mass, momentum, and energy, and demand highly resolved spatial and temporal measurements of the flow fields [3-5,12-16]. This, in turn, requires substantial advancements of data gathering techniques which are applied in canonical turbulence, where it is often sufficient to take one (or, a few) point(s) measurements of a temporal dependence of a flow field and transform it to a spatial scaling by using Taylor's hypothesis [13,17]. On data interpretation side, RT dynamics is characterized by power-laws; Likewise canonical turbulence, their accurate quantification requires substantial span of scales [15,17].

Considerable success has been achieved in the state-of-the-art experiments and in diagnostics of RTI and RT mixing [4,12-16]. Yet the problem is challenging. The question 'What are the qualitative and quantitative properties of Rayleigh-Taylor flows?' remains well open [5].

2.2.2 Experimental approach – the jelly method

Here we present the series of experiments in a broad range of setups [4,5,12,27-33]. The experiments are designed to ensure repeatable observations unambiguously answering the following questions: Is interfacial RT mixing heterogeneous and anisotropic? What is the influence of acceleration on order and disorder in RT mixing? How is RT mixing related to other accelerated flows?

Our experimental applies the jelly method Figure 3. The method is proven to be informative, robust and efficient. The flow is monitored by high-speed film and video recording and/or by a camera with an open shutter and a pulsed light source [12,27-33].

The jelly method has been developed by Meshkov, Rogachev, Zhidov, Nevmerzhitsky and colleagues in 1980s [27] and has been actively used since then [4,12,27-31]. It allows a broad range of

setups and a high repeatability for each setup. Our experiments use a jelly of aqueous gelatin solution. These jellies are made by using a standard technique. The plasticity of jelly is zero, and the jelly strength depends on the concentration of the solution. For small concentration ~4-5%, the jelly strength is ~10kPa. The system is accelerated by the gas pressure which is substantially greater than the jelly strength. To produce this pressure, we use either a compressed gas, or the products of the detonation of the acetylene-oxygen mixture. The resulting pressure is over than $\sim 10^2$ greater than the jelly strength. Under this pressure, the jelly behaves as a liquid. Jelly's transparency enables the use of optical methods [12,27-31].

In jelly experiments, we use a device in the form of a miniature 'gun' with a channel of square section $4\times 4\mathrm{cm}^2$ Figure 3 [12,28-31]. The channel is assembled from the Plexiglas plates that are $2\mathrm{cm}$ thick. The jelly layer is cast into the hole of one of the plates and is accelerated by the gas pressure. In experiments with gas pressure produced by the detonation products, initially, at temperature $300^{\circ}\mathrm{K}$ and pressure $10^5\mathrm{Pa}$, an acetylene - oxygen mixture has density $1.350\mathrm{kg/m}^3$ and detonation velocity $2450\,\mathrm{m/s}$. The detonation is initiated by the electric spark(s) at one (several) point(s). After the detonation and the damping of shock waves, the detonation products in the chamber have the pressure $\sim 1.68\mathrm{MPa}$, the temperature $\sim 3800^{\circ}\mathrm{K}$, and the adiabatic index 1.27 (Gerasimov). Typical experimental values are: The speed of $4.5\mathrm{cm}$ layer is $\sim 70\,\mathrm{m/s}$, the acceleration g is $(3\text{-}7)\times 10^4\,\mathrm{m/s}^2$, the Atwood number is $A\sim 1$, the run-time T of RTI and RT mixing is $(2.5\text{-}4)\times 10^3\,\mu s$. In experiments with compressed gas, these values are smaller. In the case of compressed gas the accelerations are more uniform, when compared to the case of detonation products.

Jelly experiments enable the systematic study of sensitivity of RT mixing to deterministic and initial conditions in a broad range of setups. Initial perturbations may include perturbations of the flow fields and perturbations of the fluid interface (that is – the jelly surface) [12].

3. Results

3.1 Theory

Rayleigh-Taylor instability develops when fluids of different densities are accelerated against their density gradients, Eqs.(1), [1-5,36]. This occurs when the flow is subject to acceleration (gravity) directed from the heavy to the light fluid, or when the fluid interface moves with an acceleration directed from the light to the heavy fluid [1-5,36]. The former case is illustrated by water flowing from an overturned cup [1-5]. The latter case is observed in experiments in shock-driven fluids and plasmas [5,16]. For a nearly planar interface, these definitions are equivalent, since the interface dynamics can be considered in a frame of reference moving with the accelerated interface [1-5,36]. In theory, to describe RT dynamics at early and at late times, one usually applies the former definition, as in Eqs.(1) [1-5,36].

3.1.1 Scale-dependent early-time linear RT dynamics

In RT dynamics, the perturbations are a superposition of standing waves [1-3]. For periodic spatially extended RT flows, theory of discrete space groups can be applied [3,8]: RT dynamics is invariant with respect to a discrete spatial group $\mathbf{G}$, whose generators are translations in the plane, rotations and reflections. These groups are also known as Fedorov's or Schoenflies' space group [36,49]. Figure 2 presents sample patterns for one-dimensional discrete space groups $p1, pm11$, and two-dimensional discrete groups $p4mm, p6mm, p2mm$. Here p stands for periodicity in one (two) direction(s), and, for each of spatial directions, 1 is for unit element, m is for mirror plane of reflection, and $n = 2,4,6$ is for n-fold axis of rotation. While there are 7 one-dimensional and 17 two-dimensional discrete space groups, only some of these groups should be considered, Figure 2. Particularly, groups relevant to structurally stable RT dynamics must have anisotropy in the acceleration direction and inversion in the normal plane, such as groups of hexagon $p6mm$, square $p4mm$, rectangle $p2mm$ in 3D, and group $pm11$ in 2D, and unlike groups $p1$ in 2D or $p3m1$ in 3D [3,8,23,53]. Irreducible representations of a relevant group are applied to describe RT flow fields, including Fourier series of the velocity and pressure fields and the interface [3,5,8,19-23,36]. For small perturbations the boundary value problem Eqs.(1) is linear, and its solution is straightforward [3,8].

3.1.2 Scale-dependent late-time nonlinear RT dynamics

Nonlinear RT flows consist of large-scale coherent structures, whose dynamics is potential, and small-scale interfacial vortical structures driven by shear [3,8]. For the large-scale dynamics, by applying the irreducible representations of the relevant group, we expand the flow fields as Fourier series; a spatial expansion is further made of the governing equations Eqs.(1) in a vicinity of a regular point at the interface, i.e., the bubble tip [8,19-21,43]. The governing equations Eqs.(1) are then reduced to a dynamical system in terms of moments and surface variables. Group theory is further applied to solve the closure problem, find regular asymptotic solutions for the dynamical system, study their stability, and identify properties of the nonlinear RTI [8,19-21,44].

Briefly, for RT coherent nonlinear dynamics, regular asymptotic solutions form a continuous family. The solutions in the family converge with the increase of the approximation order. The number of the family parameters is set by the flow symmetry. This multiplicity is associated with the singular character of interfacial dynamics, and is due to the interfacial shear. The solutions stability is analyzed. The fastest stable solution is identified as the physically significant [3,8,19-21,44].

For 3D flow with group $p4mm$, the dynamics is highly isotropic, and, near the regular point, the interface is $z^* - z_0 \sim \zeta\left(x^2 + y^2\right)$, where z_0 is the position, $v = \partial z_0 / \partial t$ is the velocity, and ζ is the principal curvature of the interface at the tip of the bubble. The bubble moves up $v > 0$ and is concaved down $\zeta < 0$. To the first order, for regular asymptotic solutions in the family the bubble velocity v depends on its principal curvature ζ, $\zeta \in \left(-|\zeta_{cr}|, 0\right)$, as

$$v/\sqrt{g/k} = \sqrt{2A}\sqrt{(-2A\,\zeta/k)}\left(9-64(\zeta/k)^2\right)\left(-48(\zeta/k)+A\left(9+64(\zeta/k)^2\right)\right)^{-1/2} \quad (2a)$$

where the wavevector is $k = 2\pi/\lambda$. The fastest stable solution is the Atwood bubble with the velocity and curvature (v_{max}, ζ_{max}) Figure 4. It has the invariant $v_{max}^2/\left((g/k)\left(8|\zeta_{max}|/k\right)^3\right) = 1$, which is a function of the wavelength and amplitude and their derivatives [8,19-21,44]. At $A = 1$, the values are $\zeta_{max} = -k/8$ and $v_{max} = \sqrt{g/k}$. The interfacial shear function near the bubble tip can be defined as the spatial derivative of the jump of tangential velocity at the interface, $\Gamma = \Gamma_{x(y)}$ with $\Gamma_{x(y)} = \partial\left[v_{x(y)}\right]/\partial x(y)$ leading to $\Gamma/v = 6k\left(9-64(\zeta/k)^2\right)^{-2}$. For $\zeta \in (-|\zeta_{cr}|, 0)$, the shear function Γ is 1-1 function on curvature ζ. The interface velocity is thus a function of the interfacial shear function Γ, Figure 4. This direct link of the interfacial dynamics to the interfacial shear provides the physics interpretation for the multiplicity of regular asymptotic solutions in RT coherent nonlinear dynamics.

For regular asymptotic solutions there is effectively no motion of the fluids away from the interface, there is intense fluid motion near the interface, and shear is present at the interface leading to the formation of interfacial vortical structures, Figure 5. The invariant properties of the physically significant solution imply that the wavelength λ and amplitude h both contribute to RT nonlinear dynamics. Furthermore, in RT flows, 3D coherent structures tend to conserve isotropy in the plane and have a discontinuous 2D-3D dimensional crossover (i.e., a transition from 2D to 3D flow) [8,19-21,44].

For 2D flow with group $pm11$, to the first order, for solutions in the family the bubble velocity v depends on its principal curvature ζ, $\zeta \in (-|\zeta_{cr}|, 0)$, with wavevector $k = 2\pi/\lambda$, as

$$v/\sqrt{g/k} = (3/2)\sqrt{(-A\,\zeta/k)}\left(1-4(\zeta/k)^2\right)\left(A(1-2(\zeta/k))^2-(1-A)(\zeta/k)\right)^{-1/2} \quad (2b)$$

The fastest stable solution is the Atwood bubble with the velocity and curvature (v_{max}, ζ_{max}). It has the invariant $(v_{max}/3)^2/\left((g/k)\left(2|\zeta_{max}|/k\right)^3\right) = 1$ which is a function of wavelength and amplitude and their derivatives [8,19-21,44]. At $A = 1$, the values are $\zeta_{max} = -k/6$ and $v_{max} = \sqrt{g/3k}$ with $\zeta_{max} \approx -1.05\lambda^{-1}$ and $v_{max} \approx 0.23\sqrt{g\lambda}$. Note that the group theory approach resolves the long-standing puzzle of nonlinear RT dynamics and reconciles with one another theories of RT dynamics in 2D single fluid flow [42,43], by identifying a broad interval of curvature values, by finding a continuous family of solutions, and by showing that the fastest stable solution in the family is well estimated by a single-mode solution [20].

3.1.3 Pattern formation and coherent structures and super-structures in RT dynamics

Group theory can be further applied to study transitions induced by the growth of spatial period(s) in RT dynamics. By employing irreducible representation of discrete space groups, we classify possible structures and super-structure occurring in Rayleigh-Taylor flows, and as well as transitions from one

pattern to another under modulations [8,22,23]. For pattern formation in RT flows, group theory [8,22,23] excellently agrees with experiments [12,46] and with the model [11,45].

For a three-dimensional flow with square group $p4mm$, group theory finds that under large-scale modulations, a transition may occur from an isotropic observable coherent structure with group $p4mm$ and periods $\boldsymbol{a}_{1(2)}$ (wavelengths $\left|\boldsymbol{a}_{1(2)}\right| = \lambda$) to an isotropic coherent super-structure with group $p4mm$ and double periods $2\boldsymbol{a}_{1(2)}$ (wavelengths $\left|2\boldsymbol{a}_{1(2)}\right| = 2\lambda$) Figure 6. This quadruple (multi-pole) interaction enables the conservation of the (quasi-) isotropy of the dynamics in the plane normal to the acceleration, whereas binary interactions may result in a loss of isotropy in the normal plane [8,22]. These results excellently agree with experiments [12] presented in our work and with experiments [46].

3.1.4 Self-similar RT mixing

Balances

In RT mixing, group theory is implemented in the momentum model, whose equations have the same scaling invariance as the governing equations [3,5,24-26,48]. In the momentum model, the dynamics of a parcel of fluid undergoing RT mixing is governed by a balance per unit mass of the rates of momentum gain, $\tilde{\mu}$, and momentum loss μ, as $\dot{h} = v$ and $\dot{v} = \tilde{\mu} - \mu$, where h is the (vertical) length scale along the acceleration $\mathbf{g}$, v is the corresponding velocity, μ ($\tilde{\mu}$) is the magnitude of the rate of loss (gain) of specific momentum in the acceleration direction [3,5,24-26].

The rate of loss (gain) of specific momentum μ ($\tilde{\mu}$) is associated with the rate of loss (gain) of specific energy ε ($\tilde{\varepsilon}$) as $\mu = \varepsilon / v$ ($\tilde{\mu} = \tilde{\varepsilon} / v$). The rate of energy gain is $\tilde{\varepsilon} = fgv$, $f = f(A)$, where function f is some function on the density ratio or the Atwood number A. Since we look for asymptotic solutions and consider specific balances (that is the balances per unit mass rather than per unit volume), the acceleration can be rescaled hereafter as $gf \to g$. The rate of energy dissipation is $\varepsilon = Cv^3 / L$, as in canonical turbulence [6,36]. Here C is the drag coefficient and is the model parameter with $C \in (0, +\infty)$. The length-scale L is the scale for energy dissipation. This scale can be horizontal, $L \sim \lambda$, or vertical, $L \sim h$, or a combination of scales, $L \sim L(\lambda, h)$ [3,5,8]. By applying Lie groups, the solution is sought.

For $L \sim \lambda$ the gains and losses are balanced, $\mu = \tilde{\mu}$ and $\tilde{\varepsilon} = \varepsilon$, and the dynamics is steady, $h \sim t\sqrt{g\lambda}$ [3,24-26]. For $L \sim h$, the rates of the gain and loss of specific momentum (energy) are balanced asymptotically $|\mu| \sim |\tilde{\mu}|$, and imbalanced algebraically, $\mu \neq \tilde{\mu}$ ($\tilde{\varepsilon} \neq \varepsilon$). The imbalance leads to self-similar RT mixing with $h \sim gt^2$ [3,24-26]. The imbalance may occur due to the growth of horizontal scale $\lambda \sim gt^2$, as predicted by the model [11,45] and theory [22,23]. It may occur when amplitude h is the dominant scale for energy dissipation. Per data [9-16], the imbalance is small, $(\tilde{\mu} - \mu)/\tilde{\mu} << 1$.

Symmetries

RT mixing has a number of symmetries, and is invariant with respect to scaling transformation, similarly to canonical turbulence. Yet, symmetries of RT mixing are distinct from those of turbulence [3,5,23-25]. Particularly, in canonical turbulence, the invariant of the scaling transformation is the rate of dissipation of specific kinetic energy $\varepsilon \sim v^3/L$ and $\varepsilon \sim v^3/L \sim v_l^3/l$, where $v\,(v_l)$ is the velocity scale at large (small) length scale $L\,(l)$ [6,36]. This invariance is compatible with existence of inertial interval and non-dissipative energy transport [6,17,24-26,48]. In RT mixing, the invariant of the scaling transformation is the rate of loss (gain) of specific momentum in the acceleration direction $\mu \sim v^2/L\,(\tilde{\mu} \sim g)$ and $\mu \sim v^2/L \sim v_l^2/l$ [3,24,25]: The momentum and energy are gained and lost at any scale, the rates of loss (gain) of specific momentum $\mu(\tilde{\mu})$ are invariant, and the rates of energy dissipation (gain) are time-dependent, $\varepsilon(\tilde{\varepsilon}) \sim g^2 t$ Table 2.

Scaling and correlations

In RT mixing the invariance of the rate of momentum loss μ, $\mu \sim v^2/L \sim v_l^2/l$, leads to the scaling of velocity $v_l/v \sim (l/L)^{1/2}$ and the Nth order structure function $\sim (l\mu)^{N/2}$. In canonical turbulence the invariance of the energy dissipation rate ε, $\varepsilon \sim v^3/L \sim v_l^3/l$, leads to the velocity scaling $v_l/v \sim (l/L)^{1/3}$ and the Nth order structure function $\sim (l\varepsilon)^{N/3}$. From these scaling exponents, the velocity correlations are stronger in RT mixing than in canonical turbulence Table 3. In RT mixing, the Reynolds number $Re = vL/\nu$ is scale-dependent, $Re \sim g^2 t^3/\nu$, and the local Reynolds number $Re_l = v_l l/\nu$ scales as $Re_l/Re \sim (l/L)^{3/1}$ leading to viscous scale $l_\nu \sim (\nu^2/\mu)^{1/3}$ with $l_\nu \sim \lambda_m$ Table 3 [3,24-26]. In turbulence, $Re_l/Re = (l/L)^{4/3}$ and $l_\nu \sim (\nu^3/\varepsilon)^{1/4}$ [6,36]. Span of scales increases with time in RT mixing $L/l_\nu \sim g t^2 (\mu/\nu^2)^{1/3}$, and is constant in turbulence $L/l_\nu \sim L(\varepsilon/\nu^3)^{1/4}$ Table 4.

Properties of fluctuations

Fluctuations are essential for turbulent systems, and their strength is expected to exceed the deterministic noise, i.e., the noise caused by the initial, external and experimental conditions. In canonical turbulence the invariance of energy dissipation rate $\varepsilon \sim v^3/L$ leads to diffusion scaling law for velocity fluctuations, $v \sim t^{1/2}$ [6,36]. In RT mixing, the invariance of the rate of momentum loss $\mu \sim v^2/L$ leads to ballistic dynamics, $v \sim t$ [3,5,24-26].

To compare the strengths of turbulent and deterministic fluctuations, consider two parcels of fluids entrained in the flow with a time-delay $\tilde{\tau}$. In canonical turbulence, turbulent velocity fluctuations $\sim (\varepsilon v \tilde{\tau})^{1/3}$ are substantially greater than the parcels' relative deterministic velocity $\sim (\varepsilon \tilde{\tau})^{1/2}$; the ratio of the fluctuating and the mean velocity velocities is constant $\sim (\varepsilon \tilde{\tau}/v^2)^{1/3}$ [6,36]. In RT mixing, turbulent

velocity fluctuations $\sim \mu\tilde{\tau}$ are comparable to the parcels' relative deterministic velocity $\sim \mu\tilde{\tau}$; the ratio of the fluctuating and mean velocities decays with time $\sim (\tilde{\tau}/t)$ [3,5,25].

We see that turbulence is a stochastic process with self-generated fluctuations insensitive to deterministic noise [6,36]. In RT mixing, fluctuations are sensitive to deterministic noise, and their strength decays with time [3,5,25,48]. This suggests that RT mixing may laminarize, similarly to other accelerated flows which have discovered the laminarization of turbulent flows in curved pipes and accelerated boundary layers [34,35], Table 5.

Dimensional analysis based spectra

In canonical turbulence, the invariance of energy dissipation rate leads to spectral density E of fluctuations of the kinetic energy $E \sim \varepsilon^{2/3} k^{-5/3}$ [6,36]. For statistically unsteady RT mixing, spectra may be a challenge to rigorously define. The dimensional analysis-based power-law spectrum for kinetic energy fluctuations is steeper in RT mixing than in Kolmogorov turbulence, $E \sim \mu k^{-2}$ Table 6 [3,25,48].

Note that in the balanced RT dynamics with $L \sim \lambda$ and moderate Reynolds number, a disordered state may appear for noisy initial conditions, with the span of scales $\sim (\lambda/\lambda_m)^{9/8}$ [3,5,25,26]. The accelerated ordered and chaotic disordered state may co-exist [3,5,25,26].

Spectra and correlations in realistic fluids

From a theoretical point of view we expect power-law functions for spectra and correlations to be displayed over the scales, which are far from the largest and the smallest scales, and which span a substantial dynamic range [3,6,36]. This implies that wave-vectors are $k \in (k_{min}, k_{max})$, with $k_{min} >> K$, $K \sim L^{-1}$, and $k_{max} >> k_\nu$, $k_\nu \sim l_\nu^{-1}$, and that the span of scales is $k_{min} << k << k_{max}$ with $lg(k_{max}/k_{min}) >> 1$. While such conditions are easy to implement in 'mathematical fluids', they may be challenging to achieve in experiments, where the values of K, k_ν are usually finite and bounded [3-6,36,48]. Hence, we may expect that in realistic fluids the functions of spectra and correlations to be influenced by processes occurring at scales $\sim L \sim K^{-1}$ and $\sim l_\nu \sim k_\nu^{-1}$. The former corresponds to long wavelengths, and is usually associated with some deterministic (initial) conditions. The latter is associated with processes occurring at small scales; its influence may lead to substantial departures from the power-laws. For instance, it may lead to compound functions combining a power-law and an exponential decay, as $\sim k^\alpha e^{-\beta k}$ with $\beta \sim k_\nu^{-1}$, so that the dynamics is self-similar for $k << k_\nu$ and is scale-dependent for $k \sim k_\nu$. This can be similar to anomalous scaling in isotropic homogeneous turbulence [17,48].

3.2 Experiment

Sub-sections 3.2.1-3.2.3 provide the details on experimental capabilities of the jelly method, the parameters of RT dynamics, and the studies of various effects on of RT mixing dynamics [12,27-31].

3.2.1 Experimental capabilities of the jelly method

The capabilities of the experimental facility and the method are outlined in Figure 3 and Table 7 – Table 10. Particularly, Figure 3 illustrates the experimental assembly with a channel of square section $4\times 4\text{cm}^2$. In the lower part of the assembly, gas pipes are seen that are used to fill the chamber with a gas mixture [12,27-31]. For typical setup in jelly experiments, the values of pressure, channel size, initial jelly layer thickness, initial gas layer thickness are given in Table 7. The dependence of jelly strength on the concentration of gelatin solution is provided in Table 8. Small 4.4% concentration gelatin solutions are used in our experiments [12,27-31]. Table 9 further presents the ratio of jelly strength to the gas pressure for the concentration 4.4% of gelatin solution [12,27-31]. In typical experimental setup the gas pressure is over $\sim 10^2$ greater than the jelly strength. Under this pressure, the jelly behaves as an incompressible fluid. Recall that the jelly is the material with zero plasticity [27]. Table 10 provides the range of values of the acceleration and the run-time in the jelly experiments [12,27-31]. Note that the experiment applies the jelly to control the initial conditions. For random initial conditions, other liquids can be used, such as water [12].

3.2.2 Effects of viscosity, compressibility and strength

Viscosity effect

A small concentration jelly behaves as a liquid under high pressures substantially exceeding the jelly strength. Since the gelatin solution is an aqueous solution of a polymer, the viscosity of this gelatin solution can be derived according to the formula $\nu/\nu_0 = 1+2.5(c/100)$ where ν is the solution viscosity, ν_0 is water viscosity, c is concentration in percent [50-52]. For $c=4.4$, the ratio is $\nu/\nu_0 = 1+2.5(c/100)=1.11$; this leads to $\nu \approx 1.11\times 10^{-6}\, m^2/s$.

Table 11 presents the characteristic length-scale $\lambda_m = \left(\nu^2/g\right)^{1/3}$ and time-scale $\tau_m = \left(\nu/g^2\right)^{1/3}$ in jelly experiments for pressure induced by the detonation products (DT) and by the compressed gas (CG) [12,27-31]. These length scales are substantially smaller than the chamber size and the experimental run-time thus allowing the implementation of substantial span of spatial and temporal scales.

Relevance of this viscosity value for RT dynamics in our experiments can also be viewed from the following tests [12,27-31]. By implementing at the interface a one-dimensional periodic perturbation and by allowing the resulting two-dimensional (2D) flow to evolve to the nonlinear regime, one can accurately measure the steady velocity of the nonlinear bubble. The measured value achieves excellent agreement with the nonlinear theory finding $v=0.23\sqrt{g\lambda}$ for 2D bubble velocity [20,42,43]. The Reynolds number in the experiment is estimated as $\text{Re} = t\left(0.23\sqrt{g\lambda}\right)\left(0.23\sqrt{g\lambda}\right)/\nu$ leading to

$\mathrm{Re} \sim 1.1 \times 10^4$ for $t = 2955 \mu s$, $\lambda = 8mm$ and $g = 10^4 \, m/s^2$. It is well known that in the simulations the Reynolds number should be large enough, $\mathrm{Re} >> 10^3$, to compare well with 2D nonlinear theory in ideal fluids [3,8]. Hence the observed dynamics in our experiments is essentially inviscid.

Compressibility effect

Similarly, we estimate the Mach number in the nonlinear RTI as $M = 0.23\sqrt{g\lambda}/c$ with the speed of sound of water $c = 1.5 \times 10^3 \, m/s$, leading to $M = 1.4 \times 10^{-3}$. This estimate can be applied since the jelly is the material with zero plasticity [12]. It is well known that in numerical simulations the Mach number should be small enough, $M << 10^{-2}$ in order to achieve good agreement with the theory finding the velocity of 2D nonlinear bubble $v = 0.23\sqrt{g\lambda}$ [20,42,43]. This clearly illustrates that the observed dynamics in our experiments is essentially incompressible [12,27-31].

Strength effect

In experiments presented in the paper we focus on experiments in gelatin solutions with small concentrations (~4%), when the flow is accelerated by the gas pressure which is substantially ($\sim 10^2 - 10^3$) greater than the jelly strength and when, under the pressure, the jelly behaves as an incompressible fluid. In other experiments, we have systematically studied the effect of material strength on the development of Rayleigh-Taylor mixing by varying the gelatin solution concentration from small (~4%) to large (~52%) values. Details are given in [12,29].

While the jelly is the material with zero plasticity, the jelly strength, and thus the concentration of the gelatin solution influence RT dynamics qualitatively and quantitatively for large values of the concentration and strengths [12,29]. Our experiments find the following. For small and intermediate concentrations (up to ~17%), the dynamics of Rayleigh-Taylor interfacial mixing is qualitatively similar to the case of the gas-liquid interface and is essentially strength-free. For large concentrations (from ~26% to 52%) the mixing flow changes its character. Particularly, in the large concentration case the gas penetrates the jelly layer in 'elongated caterpillar-like hollows' and the jelly penetrates the gas in 'walls' separating these hollows [12,29]. This quasi-two-dimensional structure differs from the traditional three-dimensional structure of bubbles and spikes in Rayleigh-Taylor mixing in strength-free materials.

Furthermore, our experiments find that in Rayleigh-Taylor mixing in strength-free materials (i.e., small concentration gelatin solutions) the 3D perturbations grow faster than the 2D perturbations, whereas in materials with strength (i.e., in large concentration gelatin solutions) the 2D perturbations grow faster than the 3D perturbations. In jelly experiments with the gelatin solution concentration ~26%, both mechanisms of the development of the Rayleigh-Taylor mixing are observed: First, the quasi-two-dimensional structure develops (with elongated caterpillar-like hollows and walls). Then, this quasi-two-dimensional structure is gradually transformed to a three-dimensional structure of nearly-isotropic bubbles and spikes [12,29].

In experiments discussed in this paper we use the jellies with small concentration gelatin solutions, and the observed dynamics is essentially strength free Table 7 – Table 9.

3.2.3 Parameters of Rayleigh-Taylor mixing

Based on the experimental parameters in Table 7 – Table 10, we can further estimate the parameters of Rayleigh-Taylor mixing in the jelly experiments. These parameters include the ranges of length scale, the Reynolds numbers, the span of spatial and temporal scales, as well as the Mach number. These parameters are derived to compare with theory of Rayleigh-Taylor interfacial mixing [3-5]. Table 11 – Table 16 present the parameters of Rayleigh-Taylor mixing in jelly experiments with small (4.4%) concentration gelatin solutions for pressure induced by the detonation products (DT) and the compressed gas (CG) [12,27-33]. The parameters values are given for the largest length-scale, which is the width of the mixing zone L, the corresponding velocity scale v, viscosity $\nu \approx 1.11\times10^{-6}\, m^2/s$, and speed of sound $c = 1.5\times10^3\, m/s$.

Span of spatial and temporal scales

Table 11 presents the characteristic length-scale $\lambda_m = \left(\nu^2/g\right)^{1/3}$ and time-scale $\tau_m = \left(\nu/g^2\right)^{1/3}$ in jelly experiments for pressure induced by the detonation products (DT) and by the compressed gas (CG), as discussed before [12,27-31]. Table 12 presents the range of the largest length-scales in experiments discussed in this work. These experiments find that the largest length scale (RT mixing zone width) is described well by the expression $L = (a/2)\left(gT^2\right)$ with $(a/2) \approx 0.075$ leading to the largest velocity scale $v = agT$ [9-12].

The value of parameter $(a/2)$ is a subject of intense numerical and experimental studies [9-12,15]. These studies find the sensitivity of the parameter $(a/2)$ to various conditions, including the effect of long wavelength perturbations in experiments and the effect of the sub-grid scale model in simulations. Particularly, the work [11] has found that 'Long-wavelength perturbations could be present in the initial data and could contribute to the self-similar growth constant [sic] by a factor of 2 or more.'

In our jelly experiments the initial conditions at the interface are straightforward to control. Certain care should be taken of how the acceleration is induced by the detonation products or by the compressed gas. In the experiments discussed in the work the value $(a/2) \sim 0.07$, which is close to the values $0.06 - 0.07$ reported in experiments [53], the value 0.078 reported in experiments [14], and the value 0.06 found in simulations [11]. We also observe that, depending on the thickness of the accelerated liquid (jelly) layer, the parameter $(a/2)$ may vary by a factor of 2, from ~ 0.075 to ~ 0.15. We believe that these variations are due to the passage of shock waves (which are induced by the detonation) through the liquid (jelly) layer [12,28-31].

Table 13 and Table 14 present the span of spatial scales L/λ_m and the span of temporal scales T/τ_m. Our experiments achieve the span of spatial scales up to four decades, and the span of temporal scales up to three decades.

Reynolds number

The Reynolds number is a basic quantity characterizing canonical turbulence. For statistically unsteady time-dependent accelerated Rayleigh-Taylor mixing, other quantities can be applied, and the Reynolds numbers can be used for estimates only.

In Table 15, the Reynolds number is derived as $Re = vL/\nu$, with $L = (a/2)(gT^2)$, $v = a(gT)$, with $(a/2) \approx 0.075$, and $\nu \approx 1.11 \times 10^{-6}\ m^2/s$, in accordance with group theory scaling $Re \sim g^2T^3/\nu$ [3,25] and in agreement with experiments [12-16]. We choose this definition of the Reynolds number to conveniently compare our experiments with one another in a broad range of set-ups. The range of the Reynolds number Re is estimated as 1.4×10^5 - 3.2×10^6 Table 15 [12,27-31]. The high values of the Reynolds number $Re \sim g^2T^3/\nu$ are enabled by the large magnitudes of the acceleration g and the long run-times T. To our knowledge, our experiments achieve one of the largest Reynolds number 3.2×10^6 in the state-of-the-art laboratory experiments on Rayleigh-Taylor dynamics [12-16]. The variations of the Reynolds number in the experiments, from $Re \sim 3.6 \times 10^5$ to $Re \sim 3.2 \times 10^6$, have effectively no influence on the major qualitative result – the direct observation of heterogeneity and anisotropy of RT mixing.

Per group theory [3,5,25], the viscous length scale λ_ν and viscous time-scale λ_ν in RT mixing are comparable to characteristic length and time scales $\lambda_\nu \sim \lambda_m$ and $t_\nu \sim \tau_m$ Table 11, whereas the spans of spatial L/l_ν and temporal scales T/t_ν are scaled with the Reynolds number as $L/l_\nu \sim Re^{2/3}$ and $T/t_\nu \sim Re^{1/3}$. Comparison of the span of scales in Table 13 and Table 14 with the values of the Reynolds number in Table 15 confirms the group theory scaling [3,5,25] in experiment [12,27-31].

Froude number

The Froude number is often applied to evaluate the effect of acceleration on fluid flows. By defining the Froude number as $Fr = v/\sqrt{gL}$ with $L = (a/2)(gT^2)$, $v = a(gT)$, $(a/2) \approx 0.075$, we find that in Rayleigh-Taylor mixing the Froude number is $Fr = \sqrt{2a}$ leading to $Fr \approx 0.548$ and suggesting that acceleration effects are essential in Rayleigh-Taylor mixing.

Mach number

Table 16 provides the range of the Mach number in the jelly experiments with low concentration gelatin solutions. The Mach number is defined as $M = v/c$, with $v = agT$, $(a/2) \approx 0.075$, $c = 1.5 \times 10^3\ m/s$. The range of the Mach number M is estimated as 1.2×10^{-3} - 2.8×10^{-2} suggesting that in the jelly experiments with low concentration gelatin solutions the compressibility effects are quantitatively small [12,27-31].

Hence the jelly experiments with the low concentration gelatin solutions enable the studies of Rayleigh-Taylor interfacial mixing at high Reynolds numbers with large spans of spatial and temporal scales for nearly incompressible fluids. We emphasize that these experiments [12] apply the jelly to fully control of the initial conditions. For random initial conditions, other liquids can be used. The principal

qualitative result of the experiments - direct observation of heterogeneity and anisotropy of RT mixing at high Reynolds numbers - holds true with the variations of the Reynolds number in few orders of magnitude [12,27-31].

3.2.4 Sensitivity of RTI and RT mixing to initial and deterministic experimental conditions

The jelly experiments are designed to enable a systematic study whether RT mixing is sensitive to initial and deterministic experimental conditions in a broad range of setups [12,27-31]. In Figure 7 – Figure 12 the interface is initially accelerated by the acceleration directed from the light to the heavy fluid such that the acceleration $\mathbf{g}$ is directed from the heavy to the light fluid. Initial perturbations may include perturbations of the flow fields and perturbations of the fluid interface. The former can be associated with the perturbations of pressure of the compressed gas and/or the detonation products. The latter can be imposed at the jelly surface, and they be periodic or localized, ordered or random [12,27-31].

Periodic perturbations of the interface

Figure 7 illustrates the development of RTI in a sample case of a periodic two-dimensional (2D) flow for a layer of jelly which is placed in a container and accelerated by compressed gas. A 2D periodic initial perturbation with very small amplitude ~5% of the perturbation wavelength is imposed initially at the jelly surface [29]. The development of RTI is compared with theory [3,8,12,20,42-44]. In experiment, the interface perturbation first grows symmetrically. When the perturbation amplitude is achieved ~40% of its wavelength, the perturbation becomes asymmetric, and the large-scale interfacial coherent structure of bubble and spikes develops. In the nonlinear RTI, the bubbles have constant velocity, $\sim 0.23\sqrt{g\lambda}$ and the spikes accelerate, in agreement with group theory and other theories and models for $A \sim 1$ [3,8,12,20,42-44]. Excellent quantitative agreement of the experiment and the theory suggests that RT dynamics which is observed in the jelly experiments is essentially incompressible and inviscid [12,27-31].

Bubbles competition under modulations

Figure 8 illustrates the transition of RT flow to accelerated RT mixing via the growth of the horizontal scales. The initial perturbation consists of 10x10 hemi-spherical hollows placed periodically on the jelly's layer surface. The acceleration is set by the pressure of detonation products. In the linear and nonlinear regimes, the dynamics is coherent, the bubbles move with the same constant velocity, and the spikes accelerate. Large-scale modulations, which are due to non-uniformities of the acceleration induced by the point detonation, trigger the interaction of bubbles. Some of the bubbles merge and grow faster than their neighbors. With time, the competition of bubbles increases, and the flow becomes more disordered. These experiments are in excellent agreement with merger model [11,45] and with group theory [3,8,22,23]. Particularly, in agreement with group theory, the transition from an ordered coherent structure to a super-structure with larger periods is triggered by large-scale modulations and occurs via multi-pole interactions of the bubbles [3,8,22,23]. A tendency of bubbles to keep a nearly isotropic shape in the plane normal to the acceleration is seen in Figure 8.

Perturbations of the flow fields and non-uniformities of the acceleration

In addition to the interface perturbations, the perturbations of the flow fields may also lead to the development of RTI. The jelly experiments enable the study of RTI caused by flow fields' perturbations.

Particularly, the initiation of a detonation wave of a gas mixture in experiments on the acceleration of a layer of jelly in a channel is carried out synchronously by an electric spark method in spark gaps (~1mm). From each of the 'initiation points' an almost spherical detonation wave propagates. When these waves collide with each other, with the walls of the channel and with the surface of the accelerated layer, the waves are reflected in the form of non-stationary shock waves, which are transverse waves, and which propagate into the detonation products of the gas mixture. Then these shock waves collide with each other, collide with the walls of the assembly, are reflected and circulate in the volume of the assembly, and gradually decay [12,28].

In the places where the detonation and the later transverse waves collide, the short-time high pressure regions occur at the unstable surface of the accelerated layer, which are the source of the initial perturbations. Due to the non-stationary character of these waves, these high pressure regions are short-time and small-scales. The interference of these waves is a source of local perturbations. Figure 9 shows the results of two experiments demonstrating different types of the perturbations which are presented by different locations of initiation points on the chamber bottom containing the gas mixture [12,28].

Figure 9 illustrates RT evolution of perturbations at the unstable surface of the initially planar jelly layer accelerated by pressure of detonation products in a channel with square section. The interface acceleration is directed from the reader, and the acceleration $\mathbf{g}$ is directed from the reader. The layer moves towards the reader. The instability develops at the boundary of the layer external to the reader. In Figure 9a the detonation is initiated at one point in the center of the bottom of the chamber. The bubble chains are formed along the symmetry axes of the unstable surface of the layer. In the center of the layer, the largest central bubble is formed at the intersection of the symmetry axes. In Figure 9b, the detonation is initiated at 8 points along a straight line. A chain of bubbles is formed on the unstable surface of the layer parallel to this straight line [12,28]. These experiments illustrate the sensitivity of RT dynamics to deterministic experimental conditions.

Localized perturbations

To further study the effect of deterministic experimental conditions on RT mixing, we consider RT dynamics of initially localized perturbations. We call the perturbations as local or localized when the perturbations of an unstable interface occupy a small area of this surface [12]. RT evolution of the localized perturbations differs from that of the periodic ones [12,28].

Figure 10a presents the development of RT mixing for a localized initial perturbation in the form of a hemi-spherical hollow at the unstable surface of the jelly layer. With time, the perturbation grows in the amplitude and widens laterally acquiring a nearly-spherical shape [12]. Figure 10b illustrates the development of RT mixing for a periodic initial perturbation in the form of the same 5x5 hollows uniformly located on the jelly layer surface. The perturbation amplitude grows, whereas the bubbles size in the transverse direction practically does not change and bubbles' merge does not occur. Further note

the development of small scale structures on the surface near a local disturbance in Figure 11a and the almost complete suppression of such structures by the growing periodic perturbation in Figure 11b.

Figure 11 shows an increase in the amplitude as $h \sim gt^2$ of the localized perturbation in the form of a small conical spike on the unstable surface of the jelly layer accelerated by the compressed gas. In this case, as time progresses, RT mixing zone develops at the initially flat liquid-gas interface along with the evolution of the localized conical spike. The size of the conical spike increases with time whereas its shape remains conical, and a certain narrowing of the cone is observed, as a slight decrease in the angle at its apex [30].

Hence according to our experimental results, in a broad range of setups, including periodic and localized perturbations of the interface and the flow fields, the development of RTI and the properties of RT mixing are sensitive to initial and deterministic experimental conditions even at high Reynolds numbers, in excellent agreement with group theory results [5]. Recall that canonical turbulence is a stochastic process independent of initial and deterministic conditions [6]. Note also that results in Figure 7 – Figure 11 agree with group theory finding that growth of horizontal scales is possible and is not a necessary condition for accelerated RT mixing to occur.

3.2.5 Heterogeneity and anisotropy of RT mixing

The jelly experiments are designed to enable a systematic study whether RT mixing is heterogeneous and anisotropic in a broad range of setups [4,12,27-33].

Planar geometry

Figure 12 illustrates the development of RT mixing at the liquid-gas interface in planar geometry. The experimental setup consists of two layers of jelly which are separated by an air gap and have flat surfaces initially. The lower layer is accelerated by the pressure ~ 1.5MPa of detonation products in the 4x4cm^2 chamber which are located in the lower part of the channel. The detonation is initiated synchronously by electric sparks at 8x8 uniformly positioned points at the bottom of the chamber. The initial perturbation at the surface of the lower layer has two components: the roughness of the layer surface and the perturbations of the detonation wave. The upper jelly layer is accelerated by the pressure of air which is compressed by the flying lower layer. The initial perturbation at this surface is set only by the surface roughness [12].

Confined geometry

Figure 13 - Figure 14 illustrate the development of RT mixing in confined geometry at the cylindrical liquid-gas interface in the regimes of explosion and implosion. In this experimental setup a 1cm jelly ring is placed between two Plexiglas plates. In Figure 13a,b, the inner volume of the ring is filled with acetylene-oxygen mixture. Its detonation is initiated by an electric spark at the chamber axis. The expansion of the ring and the development of RT mixing at the inner surface of the ring are registered by a camera with an open shutter in a darkened room when the experimental device is illuminated by a flash of light. In this case, the initial perturbation is the surface roughness of the ring. In Figure 14, the experimental assembly is consisted of two Plexiglas plates and a cylindrical shell between them. A ring of

jelly is placed inside the shell and concentrically to the shell. The volume between the shell and the jelly ring is filled with acetylene-oxygen mixture; its detonation is initiated by electric sparks at 40 points that are uniformly located along the inner surface of the shell. The detonation products pressure leads to collapse of the ring. The development of RT development at the outer surface of the ring is recorded by a high-speed camera. In this case, the initial perturbation is the surface roughness of the ring and the perturbations of the detonation wave [12].

Interfacial density jump

While the setups in experiments presented in Figure 12 – Figure 14 vary significantly (including the types of initial perturbations, accelerations, flow geometries), their results have an important qualitative feature in common. Particularly, in each of the experiments, the zone of RT mixing consists of two parts – the first dark, opaque, dispersed part adjacent to the gas, whose pressure accelerates the liquid layer (initially – jelly layer), and the second part in the form of a transparent bright bubbles penetrating into the liquid (initially - jelly). This is lucidly seen in the expanding ring experiment Figure 13b [12]. The direct observation of the light coloration of the bubbles and their transparency means that the bubbles are filled with the luminous detonation products having a very high temperature. This further means that at the dome of each bubble there is a density jump at the interface of the liquid (initially – jelly) and the gaseous detonation products. Furthermore, this jump is the jump that has existed at the interface initially. The surface of the bubbles penetrating the liquid (jelly) is the strongly deformed initial surface (between the detonation products and the jelly). The density jump at the surface of the bubble domes prevents the erosion of this liquid-gas interface. It is required for the development of the accelerated RT mixing.

Our jelly experiments study RTI and RT mixing in liquid-gas systems with high Atwood numbers, $A \approx 1$. Similar results are obtained for interfacial mixing gas-gas systems with low Atwood numbers, $A << 1$, with a slightly modified mechanism of the formation of the density jump [4,12,32]. Particularly, for a gas-gas interface, a heavier gas penetrates into the mixing zone as a mixture with a lighter gas, and the mixing zone development is carried out by the spikes of a heavy gas [4,12]. This is illustrated by Figure 15. Details of these experiments are given elsewhere [4].

Hence, according to our experimental results, RT mixing is the interfacial process with the density jump at the interface, and it remains heterogeneous and anisotropic even at very high Reynolds numbers, in agreement with group theory results. Recall that canonical turbulence is free from interfaces and is homogeneous and isotropic [12].

3.2.6 Order in RT mixing

The jelly experiments enable a systematic study whether RT mixing may keep order in a broad range of setups [3,5].

Consider in more details the evolution of the localized perturbation in the form of a small conical spike on the flat surface of the jelly layer accelerated by the compressed gas, Figure 11. Upon the acceleration, RT mixing develops at the initially flat liquid-gas interface. The conical spike also evolves, such that its amplitude grows with time as $h \sim gt^2$, its length-scale in the lateral direction also increases

quadraticcally with time, and the shape of the localized perturbation remains conical with a certain narrowing of the spike's cone [12,30]. This conical spike grows self-similarly. In order to ensure the growth of the spike's volume, a flow is required of the material of the accelerated layer. Since the liquid layer moves with an approximately constant acceleration and the length-scale of the spike increases quadraticcally with time, $\sim t^2$, this leads to the scaling $\sim t^6$ for the volume of the conical spike and thus the flow of the layer material. The appearance of the conical spike in Figure 11 suggests that this flow has a laminar character. Specifically, it is a laminar flow that penetrates the mixing zone.

Hence, according to our experimental results, depending on the initial and deterministic experimental conditions, the laminar flow may exist in accelerated RT mixing even at very high Reynolds numbers, Figure 9, Figure 11, in excellent agreement with group theory [3-5,8,12,24-26,30-32,48]. We emphasize that in our experiments the span of temporal scales is very large, $\sim 10^2$, Table 14, and the flow laminarization is due to the effect of acceleration. Laminarization of turbulent flows has been observed in strongly accelerated boundary layers and in strongly curved pipes [34,35].

3.3 Properties of RT dynamics in theory and in experiment

Our theory is based on group theory and solves the boundary value and initial value problems for scale-dependent linear and nonlinear RTI, and analyzes symmetries, invariants, correlations and spectra for self-similar RT mixing.

For scale-dependent RTI, the theory's principal results are: the list of discrete space groups enabling structural stability of coherent patterns; the multi-scale and interfacial character of nonlinear coherent dynamics, to which both the wavelength and the amplitude contribute; the tendency of RT flows to keep isotropy in the plane normal to the acceleration; the discontinuous dimensional crossover; the list of possible transitions from structures to super-structures Figure 1, Figure 2, Figure 4 – Figure 6 [3,5,8,19-23].

For self-similar RT mixing, the theory's principal results are: the new symmetries and scaling transformations; the invariance of the rate of momentum loss for the case of constant acceleration; the ordered character of RT mixing due to strong correlations and weak fluctuations, and sensitivity of RT mixing to deterministic conditions Table 1 - Table 6 [3,5,8,24-26,48].

Our experiment is designed to reliably and repeatedly observe in a broad range of setups the scale-dependent RTI and self-similar RT mixing Table 7 – Table 16, Figure 3, Figure 7 – Figure 14 [12,27-33,54,55].

The experiment finds that in a broad range of setups, including perturbations of the interface and the flow fields as well as periodic and localized perturbations, RT dynamics is sensitive to the initial and deterministic experimental conditions. Particularly, even at high Reynolds number the accelerated self-similar RT mixing remains sensitive to initial conditions and deterministic experimental conditions and is free from exhibiting (at least, well-defined) stochasticity, in agreement with group theory results Table 1-Table 15, Figure 11 – Figure 14 [3-5,12,27-33,54,55].

The experiment directly observes that the interface between the fluids does not become smeared during the development of RT mixing at even at high Reynolds numbers Figure 11 – Figure 14 [12]. The interface is strongly deformed. It is the strongly deformed initial interface between the fluids. The density jump is preserved at the interface at advanced stages of RT mixing. The existence of this jump is required for accelerated RT mixing to continuously develop. It ensures that the width of RT mixing zone increases in time at an increasing rate [3-5,12,27-31]. According to our experimental results, RT mixing is the interfacial process with a density jump at the interface. It remains heterogeneous and anisotropic at very high Reynolds numbers, in agreement with group theory results.

Our experiment finds that laminar flows may exist in RT mixing even at high Reynolds numbers Figure 11, Figure 13, Figure 14. It suggests that similarity to other accelerated flows [34,35], RT mixing may laminarize, in agreement with group theory results [3,5].

The theory and the experiment agree with one another and find: RT mixing is heterogeneous and anisotropic and is sensitive to initial and deterministic conditions. Its properties may depart from the properties of homogeneous and isotropic stochastic turbulence. Accelerated RT mixing may exhibit order and laminarize, similarly to other classical accelerated flows [3,5,12,25,34,35].

Note that our results are consistent with other fluid experiments which study the effect of turbulence on RT mixing and which are focused on fluctuations spectra [15]. These experiments observe that RT mixing spectra are steeper than those in canonical turbulence, suggesting a trend toward group theory results [15]. Substantial dynamic range can help to precisely quantify RT mixing power-laws, to be achieved in the future [15,17].

4. Discussion

We have applied theory and experiment to study Rayleigh-Taylor instability and Rayleigh-Taylor mixing. Our analysis has employed group theory and found that RT dynamics is interfacial and multi-scale, and RT mixing exhibits strong correlations and weak fluctuations, and is sensitive to deterministic conditions. Our experiment has applied jelly method and unambiguously observed in a broad range of setups that RT mixing is heterogeneous, anisotropic, and sensitive to deterministic conditions even at high Reynolds numbers. The theory and the experiment agree with one another and find that RT mixing may keep order and laminarize, similarly to other accelerated flows, Table 1 – Table 16, Figure 1 - Figure 15, Eqs.(1-2).

Our theory is harmonious with models [10,11] and turbulence theory [6,36], and is linked to turbulence models [47]. Our experiment is congruous with other experiments in RT flows [14-16,46] and accelerated flows [34,35], and has one of the largest Reynolds numbers in RT laboratory studies [4,5,7-16]. Our major qualitative result – heterogeneity, anisotropy and sensitivity to deterministic conditions of RT mixing - holds true with the Reynolds number variations in few orders of magnitude Figure 1 - Figure 15 [4,12]. Our theory and experiment agree with one another [3,5,8]. Our results indicate that further developments are required to study properties of RT mixing in realistic environments, and to better

understand the interplay of acceleration, interfacial dynamics and scale coupling at microscopic (kinetic) and macroscopic (continuous) scale, Table 1 – Table 16, Figure 1 - Figure 15, Eqs.(1-2).

One possible research area with many applications in nature and technology is RT mixing with variable acceleration [5,56]. For instance, in supernova, these studies are required to better understand whether turbulence may appear in blast-wave-driven RT dynamics and whether mechanisms other than turbulence may exist to enable the accumulation of energy at small scales and the nuclear synthesis [56]. In inertial confinement fusion (ICF), these investigations are in need to find new opportunities for control of RT mixing in high energy density plasmas (HEDP) [57].

Our theory suggests the following scenario for the evolution of RTI and RT mixing [3,8]: Initially, small-scale structures at the interface grow quickly. The nonlinear dynamics is interfacial and multi-scale, with the wavelength and amplitude contributing Eqs.(2) Figure 4, Figure 5. In accelerated RT mixing, the Reynolds number increases, yet RT mixing may keep order due to its strong correlations, weak fluctuations and sensitivity to deterministic conditions Table 1 – Table 6 [3,5,8,19-26,44,48]. Our experiment supports this scenario [4,12,27-33,54,55]. If the scenario holds true for variable accelerations, then in ICF, it may be worth to scratch the target in order to pre-impose proper deterministic conditions and to gain better control on RT mixing in HEDP plasma flow [3,5,56,57]. This may help the existing methods, which assume that RTI, once it appears, cannot be controlled, and leads to fully turbulent RT mixing, which are focused on the fine polishing of ICF targets in order to fully eliminate RTI [56].

The other possible research area is RT dynamics in miscible fluids. It is often believed that RT mixing of miscible fluids may lead to canonical turbulence [10,18,47]. In our experiments on RT mixing in miscible fluids, the interface is observed to be important whether the fluids are gases or liquids [4,12]. In the theory, the interface evolution with the interfacial mass flux transport requires the solution of the boundary value problem, has the inertial stabilization mechanism, and may be destabilized when the acceleration magnitude exceeds a threshold leading to the new fluid instability [58]. Further investigations to better understand the accelerated interfacial dynamics with interfacial scalar fluxes [58].

Our theory and our experiment indicate that depending on deterministic conditions a disordered (quasi-turbulent) and an ordered (laminar) dynamics may co-exist in RT flows, especially at moderate-to-high Reynolds numbers [3,5,24-26,48]. Studies of other flows (such as unsteady turbulent boundary layers, turbulent jets, and unstably stratified free shear flows) at various Reynolds numbers, Atwood and Schmidt numbers, and acceleration patterns may shed more light on the interplay of acceleration and turbulence [15,35,47].

In the studies of turbulence effect on RT mixing, spectra are common to diagnose [15,47,48]. In turbulence, these measurements are a reliable information source [13,17,36]. In RT mixing, mathematically, spectra may be a challenge to rigorously define due to statistical unsteadiness of the dynamics [3]. Physically, canonical turbulence can be viewed as a stochastic process insensitive to deterministic conditions [6,36], whereas RT mixing is sensitive to initial and deterministic experimental conditions [3,25]. Further studies are required to understand complexity and stochasticity of RT flows.

Our theory identifies a number of benchmarks to quantify RT dynamics. Some of them can be obtained from existing data, such as steeper than Kolmogorov spectra [15]. Some others require substantial improvements of diagnostics techniques to measure with high accuracy and precision, in space and in time, multiple and time-dependent scales in a single experimental run, and to augment it with high reproducibility of acceleration history and with accurate control of initial and boundary conditions and other experimental parameters [3,7]. Modern technologies can provide the experiments with principal improvements in precision, reproducibility, motion-control accuracy, dynamic range, data-acquisition rate and information capacity to better understand RT flows in realistic environments and to unambiguously compare the experimental results with rigorous theory and with simulations [13].

To conclude, we have studied theoretically and experimentally RTI and RT mixing and have found that accelerated heterogeneous anisotropic interfacial RT mixing may keep order. These results are consistent with the classical observations of the laminarization of accelerated flows and the intermittency and multi-fractality of canonical turbulence in the presence of interfaces [17,34,35]. Further investigations are required to fully understand the interplay of turbulence, acceleration, and interfacial dynamics in broad parameter regimes. The problem of water flowing from an overturned cup is a source of inspiration for researchers in science, mathematics and engineering, and is well open for a curious mind.

5. Acknowledgements

SIA thanks the National Science Foundation (USA) and the University of Western Australia (AUS).

6. References

1. Rayleigh Lord 1883 Proc London Math Soc 14, 70.
2. Taylor GI 1950 Proc R Soc A 201, 192; Davies RM, Taylor GI 1950 Proc R Soc London A 200, 375.
3. Abarzhi SI 2010 Phil Trans R Soc A 368, 1809.
4. Meshkov EE 2013 Phil Trans R Soc A 371, 20120288.
5. Anisimov SI, Drake RP, Gauthier S, Meshkov EE, Abarzhi SI 2013 Phil Trans R Soc A 371, 20130266.
6. Kolmogorov AN 1941 Dokl Akad Nauk SSSR 30, 299–303; Dokl Akad Nauk SSSR 32, 19–21.
7. Abarzhi SI, Gauthier S, Sreenivasan KR 2013 Turbulent mixing and beyond: non-equilibrium processes from atomistic to astrophysical scales. R Soc ISBN- 978-1782520382, 978-0854039869.
8. Abarzhi SI 2008 Physica Scripta 2008, 297681.
9. Kadau K, Rosenblatt C, Barber JL, Germann TG, Huang Z, Carles P, Alder BJ 2007 PNAS 104, 7741.
10. Youngs DL 2013 Phil Trans R Soc A 371, 20120173.
11. Glimm J, Sharp DH, Kaman T, Lim H 2013 Phil Trans R Soc A 371. 20120183.
12. Meshkov EE 2006 Studies of Hydrodynamic Instabilities in Laboratory Experiments (in Russian), Sarov, FGUC-VNIIEF, ISBN 5-9515-0069-9.
13. Orlov SS, Abarzhi SI, Oh S-B, Barbastathis G, Sreenivasan KR 2010 Phil Trans Roy Soc A 368, 1705.
14. Kucherenko YA et al 2003 Laser Part Beams 21, 381; Laser Part Beams 21, 369.
15. Akula B, Suchandra P, Mikhaeil M, Ranjan D 2017 JFM 816, 619.
16. Robey HF et al 2003 Phys Plasmas 10, 614.
17. Sreenivasan KR 1999 Rev Mod Phys 71, S383-S395.
18. Neuvazhaev VE 1975 Soviet Physics Doklady, 20, 398.
19. Abarzhi SI 1996 JETP 83, 1012.
20. Abarzhi SI 1998 Phys Rev Lett 81 337–40.
21. Abarzhi SI, Nishihara K, Glimm J 2003 Phys Lett A 317, 470.
22. Abarzhi SI 2008 Physica Scripta 78, 015401.
23. Pandian A, Stellingwerf RF, Abarzhi SI 2017 Physical Review Fluids 2, 073903.
24. Abarzhi SI, Gorobets A, Sreenivasan KR 2005 Phys Fluids 17, 081705.
25. Abarzhi SI 2010 Europhysics letters, 91, 35000.
26. Abarzhi SI, Rosner R 2010 Physica Scripta T142, 014012.
27. Volchenko OI, Zhidov IG, Klopov BA, Meshkov EE, Popov VV, Rogachev VG, Tolshmyakov AI 1983 Method for modeling unsteady flows of incompressible fluid // Author's certificate of the USSR #1026154 (in Russian).
28. Volchenko OI, Zhidov IG, Meshkov EE, Rogachev VG 1989 Letters ZhTF 15, 47 (in Russian).
29. Bliznetsov MV et al 1999 Proc 7th IWPCTM Russia Edited by Meshkov et al, 2.
30. Meshkov EE et al 1999 Proc 7th IWPCTM Russia Edited by Meshkov et al, 95.
31. Meshkov EE et al 1995 Proc 5th IWPCTM USA Edited by Youngs et al, 243.
32. Meshkov EE, Nikiforov VV, Toshmyakov AI 1990 Fizika Goreniya i Vzryva 3, 71 (in Russian).
33. Meshkov EE 2017 Proc of 6th Int Conf 'Turbulent Mixing and Beyond' ISBN 978-92-95003-60-6.

34. Taylor GI 1929 Proc Roy Soc A 124, 243.
35. Narasimha R, Sreenivasan KR 1973 J Fluid Mechanics 61, 417.
36. Landau LD, Lifshitz EM 1987 Course on Theoretical Physics I-X. Pergamon Press, New York.
37. Clay Institute Millennium Problems, http://claymath.org/millennium-problems.
38. Chandrasekhar S 1981 Hydrodynamic and Hydromagnetic Stability, 3d ed Dover, New York.
39. Kull HJ 1991 Theory of Rayleigh–Taylor instability Phys Rep 206 197.
40. Gauthier S, Creurer B Le 2010 Phil Trans R Soc A 368, 1681.
41. Nishihara K et al 2010 Phil Trans Roy Society A 368, 1769.
42. Garabedian PR 1957 Proc.R.Soc. A 241, 423.
43. Inogamov NA 1992 JETP Lett. 55, 521.
44. Abarzhi SI, Nishihara K, Rosner R 2006 Phys Rev E 73, 036310.
45. Glimm J, Sharp DH 1990 Phys Rev Lett 64, 2137.
46. Lugomer S 2019 Physica Scripta 94, 01500.
47. Dimotakis PE 2000 JFM 409, 69.
48. Sreenivasan KR Abarzhi SI 2013 Phil. Trans. Roy. Soc. A 371, 20130167.
49. Shubnikov AV, Koptsik VA 1974 Symmetry in science and art. Springer. ISBN 978-1468420692.
50. Einstein A 1911 Ann. Physik 34, 591.
51. Goncalves AD, Alexander C, Roberts CJ, et al. 2016 Royal Soc. Chemistry Advances 3, 15143.
52. Fishberg EH 1930 J Biol. Chem. 465, 75.
53. Kucherenko Yu et al. 1991 Proc. 3rd IWPCTM. France. p.427.
54. Meshkov EE et al 1999 Proc 7th IWPCTM Russia Edited by Meshkov et al, p.89
55. Meshkov EE, Nevmerzhitsky NV 1991 Proc 3rd IWPCTM, France, 467
56. Swisher N et al 2015 Phys Plasmas 22, 102707.
57. Haan SW et al 2011 Phys Plasmas 18, 082701.
58. Abarzhi et al 2018 PNAS:201714500. https://doi.org/10.1073/pnas.1714500115
59. Kistovich YV, Chashechkin YD 2001 Doklady-Physics 46, 718-721.
60. Chashechkin YD, Baydulov VG, Kistovich AV 2003 Comp Fluid Dynamics J 11, 480-485.
61. Abarzhi et al 2018 PNAS:201714502115. https://doi.org/10.1073/pnas.1714502115
62. Ilyin et al 2018 Phys Plasmas 25, 112105. https://doi.org/10.1063/1.5008648
63. Lugomer S 2016 Laser Part Beams 34, 123; 2017 Laser Part Beams 35, 597.

7. Tables

7.1 Theoretical tables

Table 1: Symmetries of RT mixing.

Process	Symmetries
Kolmogorov turbulence	Galilean invariance; translations in time; translations, rotations and reflections in space; scaling transformation with $L \to LK$, $v \to vK^n$, $t \to tK^{1-n}$, $\nu \to \nu K^{1+n}$.
RT mixing	Non-inertial dynamics; translations, rotations and reflections in the plane normal to gravity; scaling transformation with $L \to LK$, $t \to tK^{1-n}$, $v \to vK^n$, $\nu \to \nu K^{1+n}$, $g \to gK^{2n-1}$.

Table 2: Exponent and invariant of scaling transformations

Process	Scaling exponent	Invariant
Kolmogorov turbulence	$n = 1/3$	$\varepsilon \sim v^3/L \sim v_l^3/l$
RT mixing	$n = 1/2$	$\mu \sim v^2/L \sim v_l^2/l$

Table 3: Scaling for velocity and for velocity structure function.

Process	Velocity scaling	Structure function
Kolmogorov turbulence	$v_l/v \sim (l/L)^{1/3}$	$\sim (l\varepsilon)^{N/3}$
RT mixing	$v_l/v \sim (l/L)^{1/2}$	$\sim (l\mu)^{N/2}$

Table 4: Scaling for Reynolds number, viscous scale, and span of scales.

Process	Reynolds number scaling	Viscous scale	Span of scales
Kolmogorov turbulence	$Re_l/Re = (l/L)^{4/3}$	$l_\nu \sim (\nu^3/\varepsilon)^{1/4}$	$L/l_\nu \sim L(\varepsilon/\nu^3)^{1/4}$
RT mixing	$Re_l/Re = (l/L)^{3/2}$	$l_\nu \sim (\nu^2/\mu)^{1/3}$	$L/l_\nu \sim gt^2(\mu/\nu^2)^{1/3}$

Table 5: Fluctuations by turbulence and by deterministic conditions.

Process	Deterministic noise	Turbulent noise	Fraction of turbulent noise
Kolmogorov turbulence	$\sim (\varepsilon\tau)^{1/2}$	$\sim (\varepsilon v\tau)^{1/3}$	$\sim (\varepsilon\tau/v^2)^{1/3}$
RT mixing	$\sim \mu\tilde{\tau}$	$\sim \mu\tilde{\tau}$	$\sim \tilde{\tau}/t$

Table 6: Dimensional analysis based spectra of the fluctuations of specific kinetic energy.

Process	Spectral density	Spectral density
Kolmogorov turbulence	$E \sim \varepsilon^{2/3} k^{-5/3}$	$E \sim \varepsilon\omega^{-2}$
RT mixing	$E \sim \mu k^{-2}$	$E \sim \mu^2\omega^{-3}$

7.2 Experimental tables

Table 7: Pressure values, channel size, initial jelly layer thickness, initial gas layer thickness in typical setup in jelly experiments. Small 4.4% concentration gelatin solutions are used in these experiments.

Pressure source	Pressure	Jelly layer thickness	Gas mixture layer thickness	Square section size
Detonation products	~1.68 MPa	2cm	4cm	$4\times4\text{cm}^2$
Compressed gas	~0.25 MPa	2cm	8cm	$8\times8\text{cm}^2$

Table 8: Dependence of jelly strength on concentration of gelatin solution. Small 4.4% concentration gelatin solutions are used in these experiments.

Solution concentration	Jelly strength
4-5%	~ 10kPa
35%	~ 280kPa

Table 9: Ratio of jelly strength to gas pressure for gelatin solution concentration 4.4%.

Pressure source	Ratio
Detonation products	$\sim 5.95\times10^{-3}$
Compressed gas	$\sim 4\times10^{-2}$

Table 10: Range of accelerations and of run-time values in typical setups in jelly experiments.

Pressure source	Acceleration g_{min}	Acceleration g_{max}	Run-time T_{min}	Run-time T_{max}
Detonation products	$\sim 3.0\times10^4\ \text{m/s}^2$	$\sim 7.0\times10^4\ \text{m/s}^2$	$\sim 2.5\times10^3\ \mu s$	$\sim 4\times10^3\ \mu s$
Compressed gas	$\sim 4.8\times10^3\ \text{m/s}^2$	$\sim 8.0\times10^3\ \text{m/s}^2$	$\sim 2.5\times10^3\ \mu s$	$\sim 3.5\times10^3\ \mu s$

Table 11: Length-scale $\lambda_m=\left(\nu^2/g\right)^{1/3}$ and time-scale $\tau_m=\left(\nu/g^2\right)^{1/3}$ in jelly experiments for pressure induced by the detonation products (DT) and by the compressed gas (CG) with $\nu\approx1.11\times10^{-6}\ m^2/s$.

	g_{min}	g_{max}		g_{min}	g_{max}
DP	$\lambda_m\sim3.5\mu m$	$\lambda_m\sim2.6\mu m$	CG	$\lambda_m\sim6.4\mu m$	$\lambda_m\sim5.4\mu m$
	$\tau_m\sim11\mu m$	$\tau_m\sim6.1\mu m$		$\tau_m\sim36\mu m$	$\tau_m\sim26\mu m$

Table 12: Length-scale $L=(a/2)(gT^2)$, $(a/2)\approx0.075$.

DP	g_{min}	g_{max}	CG	g_{min}	g_{max}
T_{min}	$1.4cm$	$3.6cm$	T_{min}	$2.3mm$	$4.4mm$
T_{max}	$3.3cm$	$8.4cm$	T_{max}	$3.8mm$	$7.4mm$

Table 13: Span of spatial scales L/λ_m, with $L=(a/2)(gT^2)$, $(a/2)\approx 0.075$, $\lambda_m=(\nu^2/g)^{1/3}$, $\nu\approx 1.11\times10^{-6}\,m^2/s$

DP	g_{min}	g_{max}	CG	g_{min}	g_{max}
T_{min}	4.1×10^{3}	1.2×10^{4}	T_{min}	2.2×10^{3}	6.1×10^{3}
T_{max}	1.0×10^{4}	2.4×10^{4}	T_{max}	5.7×10^{3}	1.3×10^{4}

Table 14: Span of temporal scales T/τ_m, with $\tau_m=(\nu/g^2)^{1/3}$, $\nu\approx 1.11\times10^{-6}\,m^2/s$

DP	g_{min}	g_{max}	CG	g_{min}	g_{max}
T_{min}	2.3×10^{2}	3.7×10^{2}	T_{min}	6.8×10^{1}	9.6×10^{1}
T_{max}	4.1×10^{2}	6.6×10^{2}	T_{max}	6.9×10^{1}	1.4×10^{2}

Table 15: Reynolds numbers estimate with $Re=vL/\nu$, $L=(a/2)(gT^2)$, $v=a(gT)$, $(a/2)\approx 0.075$, $\nu\approx 1.11\times10^{-6}\,m^2/s$

DP	g_{min}	g_{max}	CG	g_{min}	g_{max}
T_{min}	1.4×10^{5}	7.8×10^{5}	T_{min}	3.6×10^{3}	1.0×10^{5}
T_{max}	5.8×10^{5}	3.2×10^{6}	T_{max}	1.0×10^{5}	2.8×10^{5}

Table 16: Mach numbers estimates with $M=v/c$, $v=agT$, $(a/2)\approx 0.075$, and c - the speed of sound.

DP	g_{min}	g_{max}	CG	g_{min}	g_{max}
T_{min}	7.5×10^{-3}	1.2×10^{-2}	T_{min}	1.2×10^{-3}	1.7×10^{-3}
T_{max}	1.8×10^{-2}	2.8×10^{-2}	T_{max}	2.0×10^{-3}	2.8×10^{-3}

8. Figure Captions

Figure 1: Schematics of the large-scale coherent structure of bubbles and spikes in Rayleigh-Taylor instability: λ is the horizontal scale (wavelength or period), h is the vertical scale (amplitude), $\mathbf{g}$ is the acceleration, $\rho_{h(l)}$ is the density of the heavy (light) fluid in the (x,z) plane. Arrows mark the direction of the fluid motion near the tip of the bubble (up) and spike (down). Small-scale interfacial vortical structures (not shown) may result in a mushroom-typed shape of the spike.

Figure 2: Sample patterns for (a) one-dimensional discrete groups $p1, pm11$, and (b) two-dimensional discrete groups $p2mm, p4mm, p6mm$. Here p stands for periodicity in one (two) direction(s), and, for each of spatial directions, 1 stands for unit element, m stands for mirror plane of reflection, and $n = 2,4,6$ stands for n-fold axis of rotation. Translation vector(s) is (are) $\boldsymbol{a}_{1(2)}$: $|\boldsymbol{a}_{1(2)}| = \lambda$ for groups $p1, pm11, p4mm, p6mm$; $|\boldsymbol{a}_{1(2)}| = \lambda_{x(y)}$ for group $p2mm$.

Figure 3: Experimental assembly with a channel of square section $4\times 4\text{cm}^2$. In the lower part of the assembly, gas pipes are seen that are used to fill the chamber with a gas mixture.

Figure 4: One parameter family of regular asymptotic solution for 3D nonlinear RTI with symmetry group $p4mm$ at some Atwood numbers A. (a) Dependence of the bubble velocity on the bubble curvature. (c) Dependence of the bubble velocity on the shear function.

Figure 5: Qualitative velocity field for incompressible inviscid immiscible fluids for a solution of the one-parameter family. (a) 3D flow with symmetry group $p4mm$. (b) 2D flow with symmetry group $pm11$. There is effectively no fluid motion away from the interface, there intense motion of the fluids near the interface, the velocity field is potential in the bulk of each fluid, the vortical structures are produced by shear at the interface.

Figure 6: Pattern formation for a large-scale coherent structure periodic in the plane under the influence of modulations. Transition is illustrated from a coherent structure with discrete space group $p4mm$ to a super-structure with discrete space group $p4mm$ with doubled periods (wavelengths). Black rhombs mark identical positions, white rhombs mark lost translations, dot-dashed lines marks the planes of reflection, and black dots marks the position of rotation axes. Dashed squares correspond to the structure, solid squares correspond to the super-structure, dashed circles mark the bubbles in the structure, and solid circle marks the bubble in super-structure.

Figure 7: Development of the periodic 2D perturbation with wavelength $\lambda = 8mm$ at the surface of the jelly layer placed in a transparent container in the channel of the square section $8\times 8\text{cm}^2$ and accelerated at $\sim 10^4\, m/s^2$ by the compressed air. The liquid-gas interface is unstable, and the perturbation of the interface rapidly increases. The time is counted from the beginning of the container movement.

Figure 8: Development of the periodic 3D perturbation at the surface of the jelly layer accelerated by the pressure of detonation products of the gas mixture in a channel with square section $4\times 4\text{cm}^2$. The initial perturbation is in the form of periodic $10\times 10=100$ hemispherical hollows on the unstable surface of the jelly layer accelerated by the pressure of the detonation products. The liquid-gas interface is unstable, and the bubble competition is triggered by large-scale modulations due to point detonation. The accelerated layer moves towards the reader. The flow registration is carried out through the accelerated transparent liquid layer. The source of light is the luminescence of detonation products.

Figure 9: Development of perturbations on the unstable surface of the jelly layer accelerated by the pressure of detonation products in a channel with square section $4\times 4\text{cm}^2$. The accelerated liquid layer moves towards the reader. The instability develops on the liquid-gas interface of the accelerated layer. The accelerated layer moves towards the reader. The interface acceleration is directed toward the reader. The acceleration $\mathbf{g}$ is directed from the reader. The flow registration is carried out through the transparent liquid layer. (a) Detonation is initiated at one point in the center of the bottom of the chamber. (b) Detonation is initiated at 8 points along a straight line.

Figure 10: RT dynamics developing at the liquid-gas interface of the accelerated layer. (a) Localized perturbation in the form of hemispherical hollow. (b) Periodic perturbation in the form of $5\times 5=25$ hemispherical hollows are imposed initially on the surface of the accelerated jelly layer accelerated by the detonation products.

Figure 11: RT dynamics developing at the liquid-gas interface of the accelerated layer. A localized perturbation in the form of a conical projection is imposed initially at the unstable flat surface of a layer of jelly accelerated by a compressed gas.

Figure 12: The development of RT mixing at the unstable liquid-gas interfaces for the experimental setup consisting of two layers of jelly which are separated by air and have initially flat surfaces. The lower layer is accelerated by the pressure of the detonation products (DP), and the upper layer - by the pressure of the air compressed by the accelerated lower layer.

Figure 13: RT mixing at liquid-gas interface in the case of explosion developing at the inner surface of the jelly ring under the pressure of the detonation products of the acetylene-oxygen mixture. (a) Preview frame: Jelly ring is placed between two plates of Plexiglas; the inner volume of the ring is filled with a mixture of acetylene and oxygen; the detonation is initiated at the center by a spark. (b) Snapshot of a flying ring at about a time when the RT mixing front comes out onto the ring outer surface.

Figure 14: RT mixing at liquid-gas interface in the case of implosion developing at the outer surface of the jelly ring under the pressure of the detonation products of the acetylene-oxygen mixture. Collapse of the jelly ring under the pressure of products of detonation (D) initiated at 40 points on the inner surface of the cylindrical case (outside the frame). In the initial stage of the collapse of the shell, RT mixing (RTM) zone is formed at the outer boundary, and in the deceleration stage at the inner boundary.

Figure 15: RT mixing at gas-gas interface at advanced stages of the evolution: The interface is between the air (with smoke impurity) and helium is clearly seen.

Figure 1

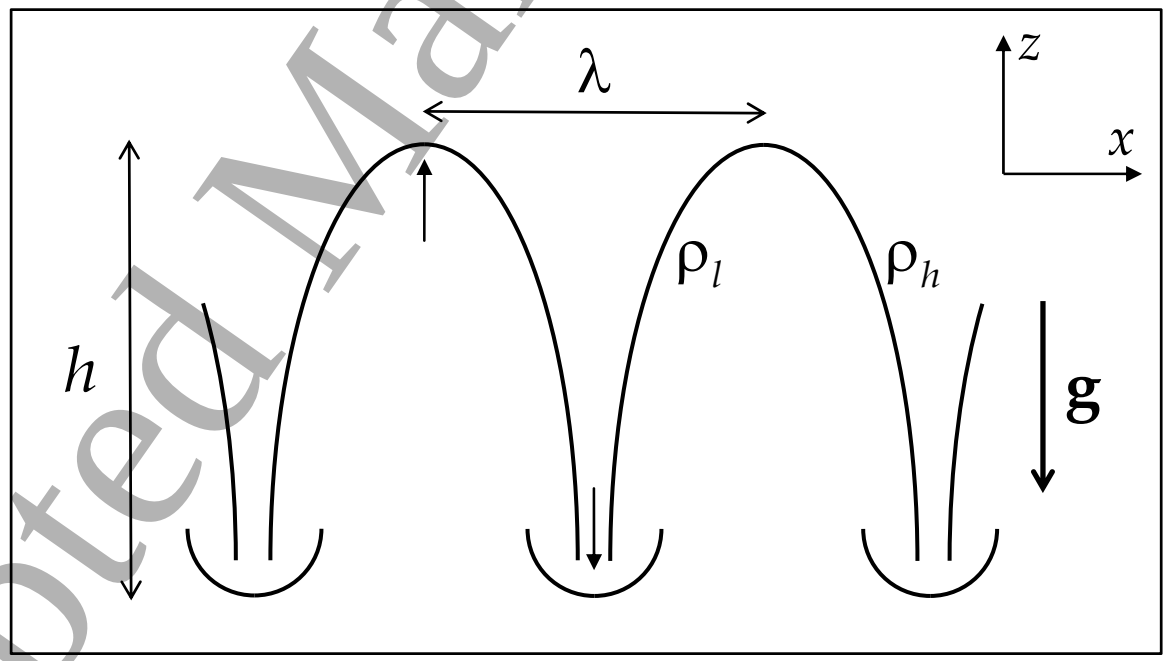

Figure 2

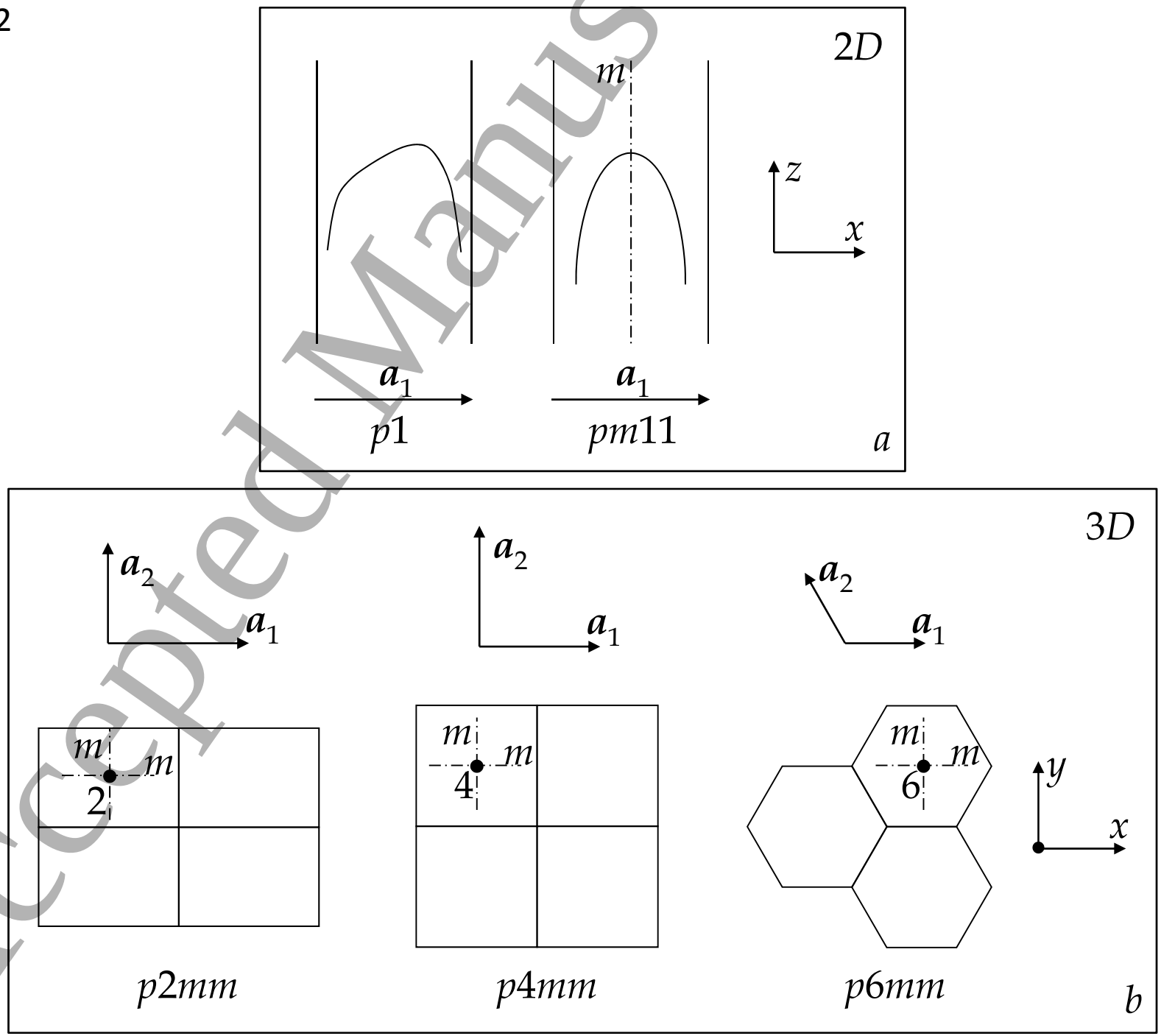

Figure 3

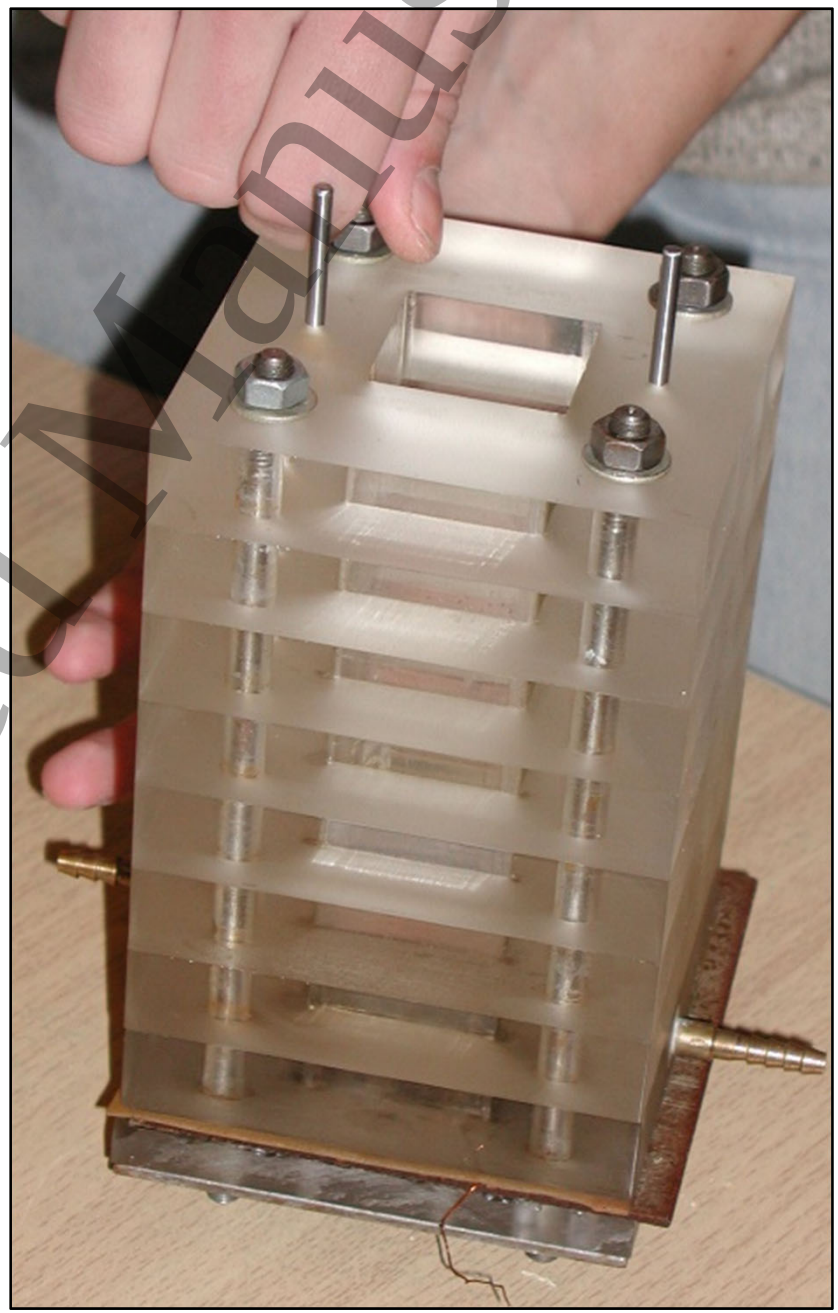

Figure 4

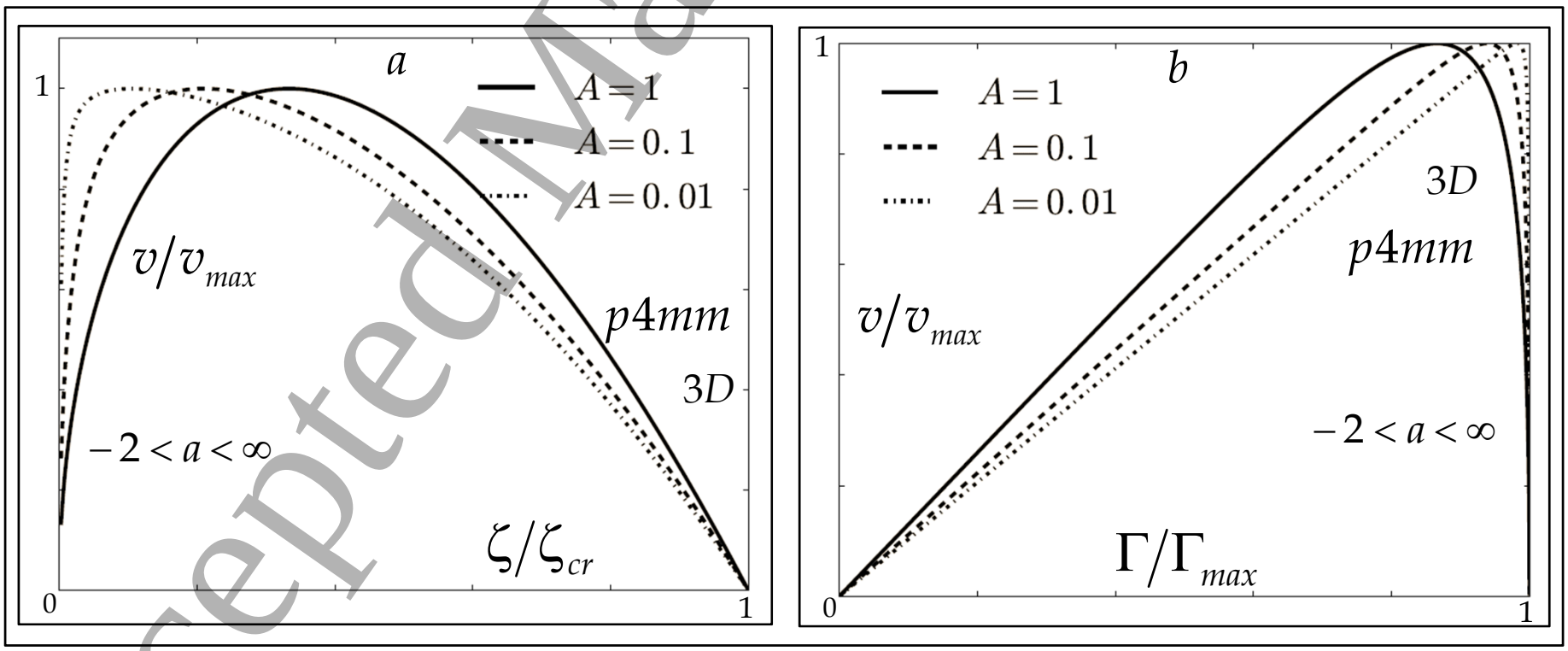

Figure 5

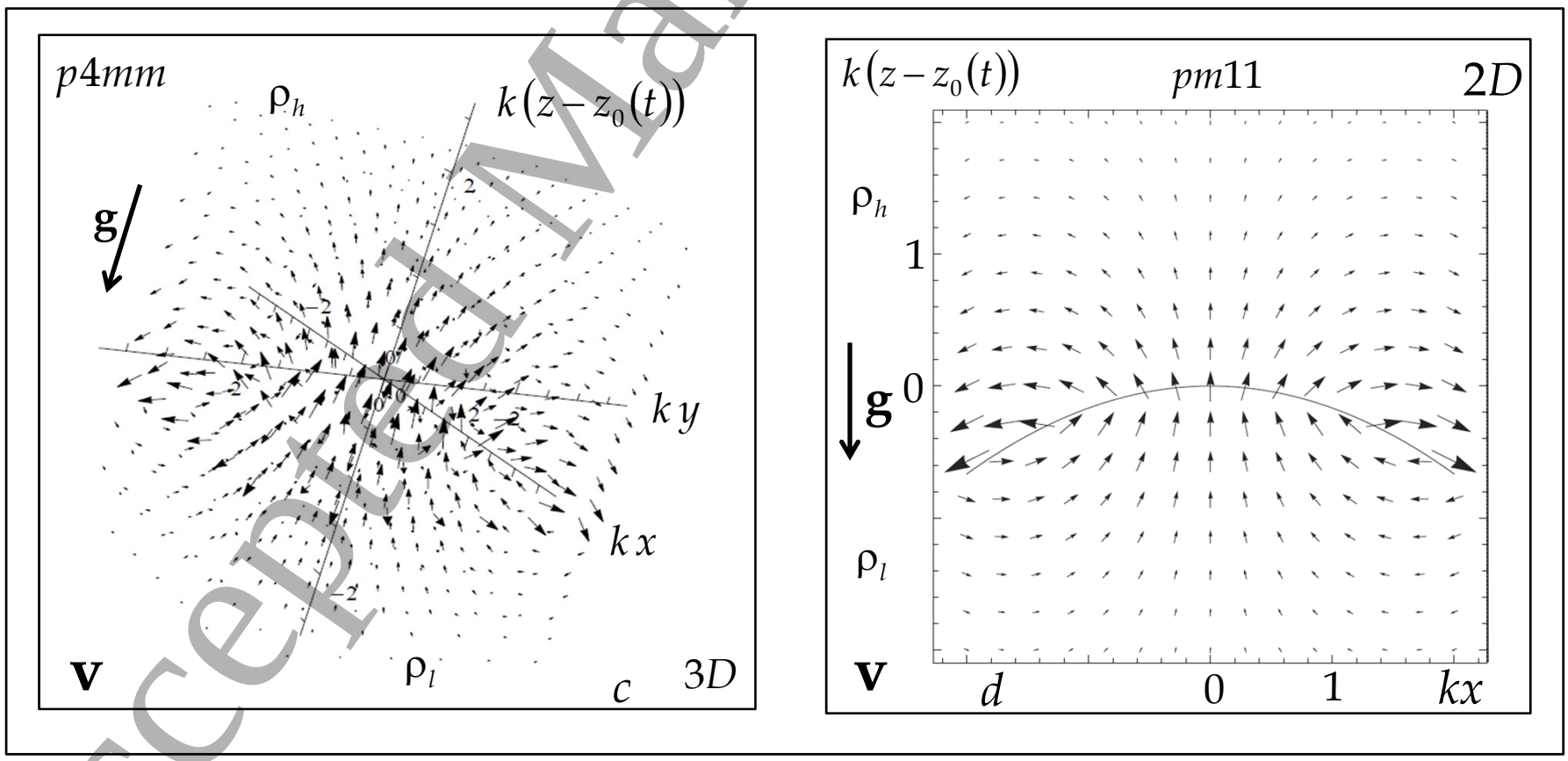

Figure 6

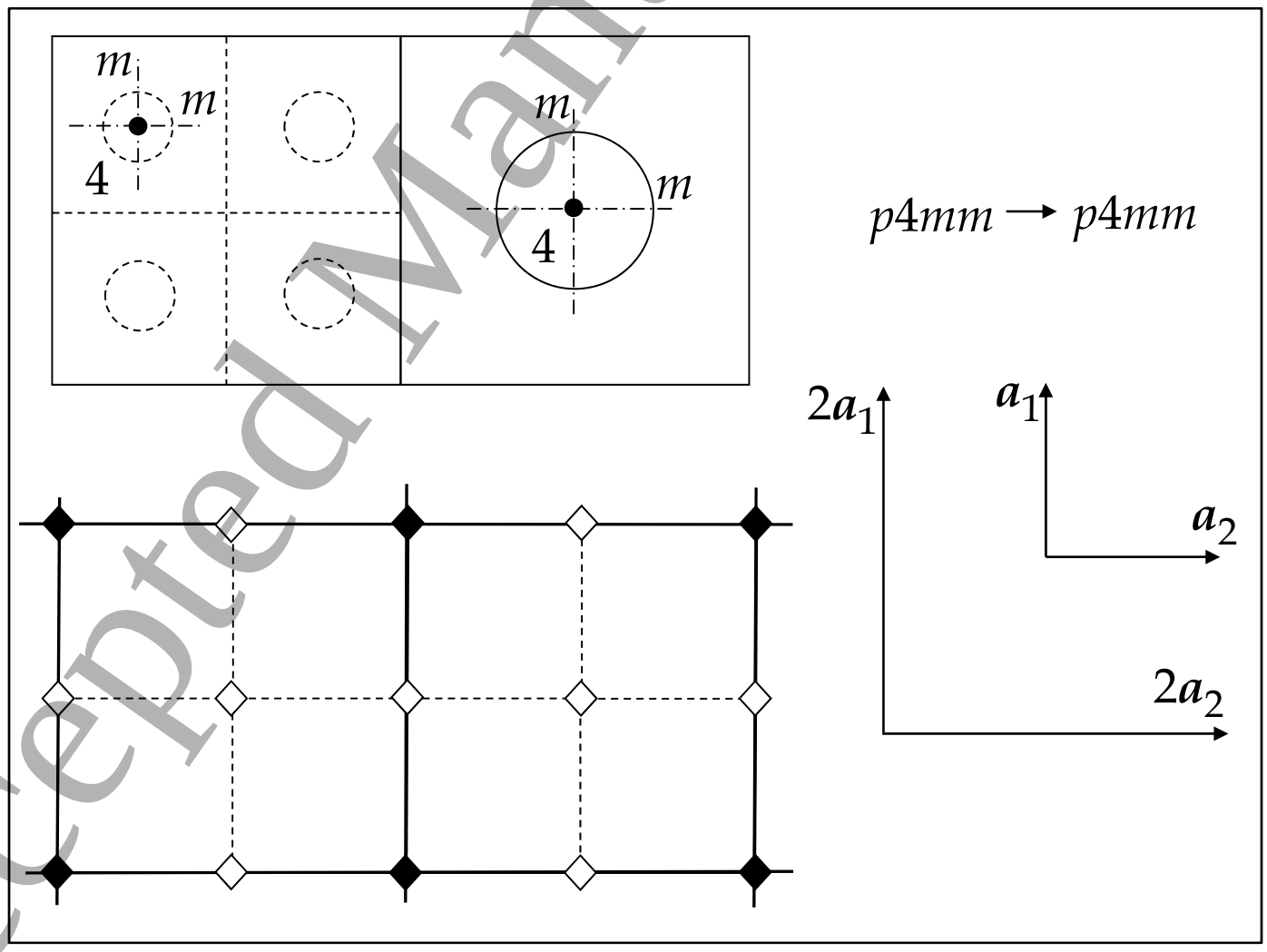

Figure 7

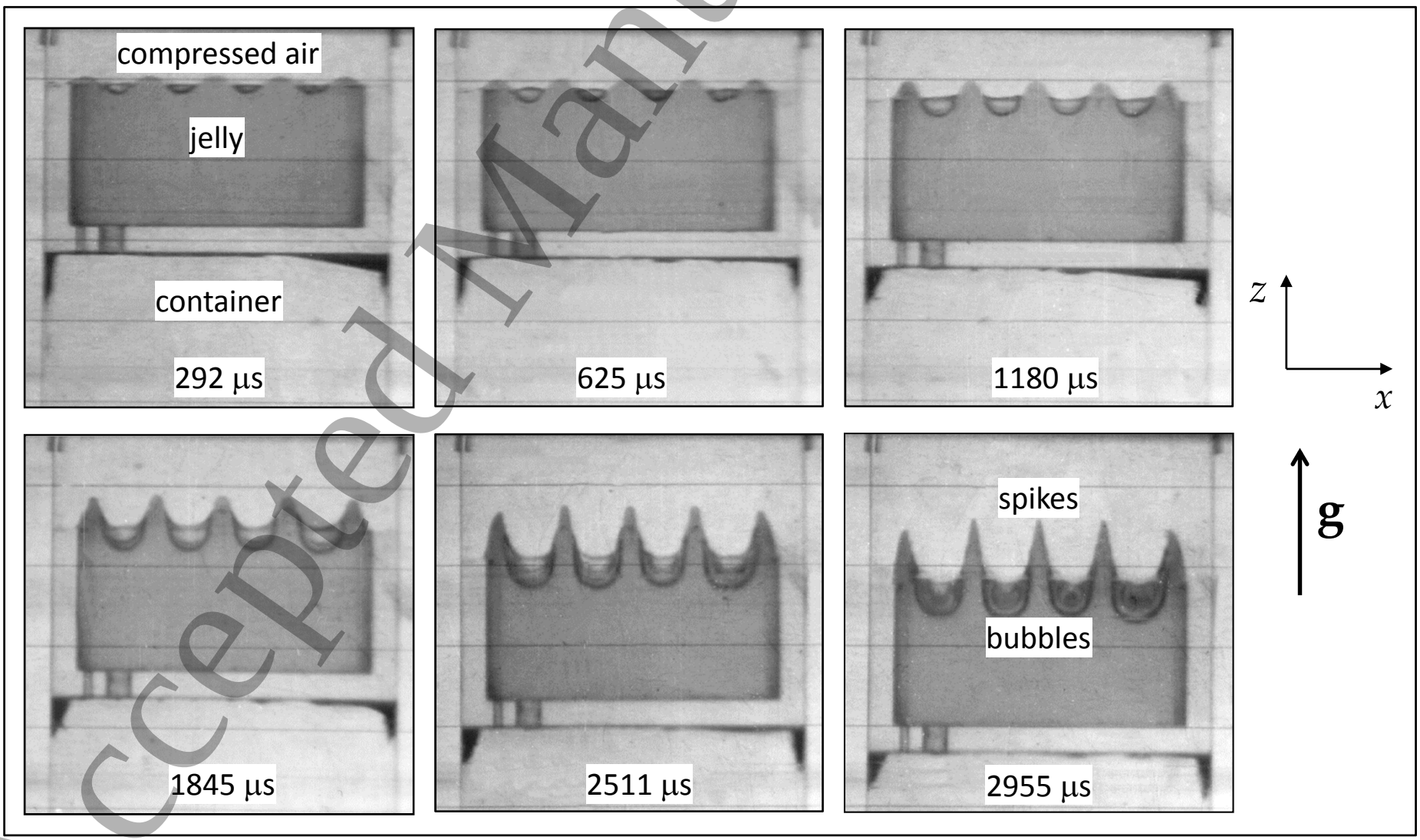

Figure 8

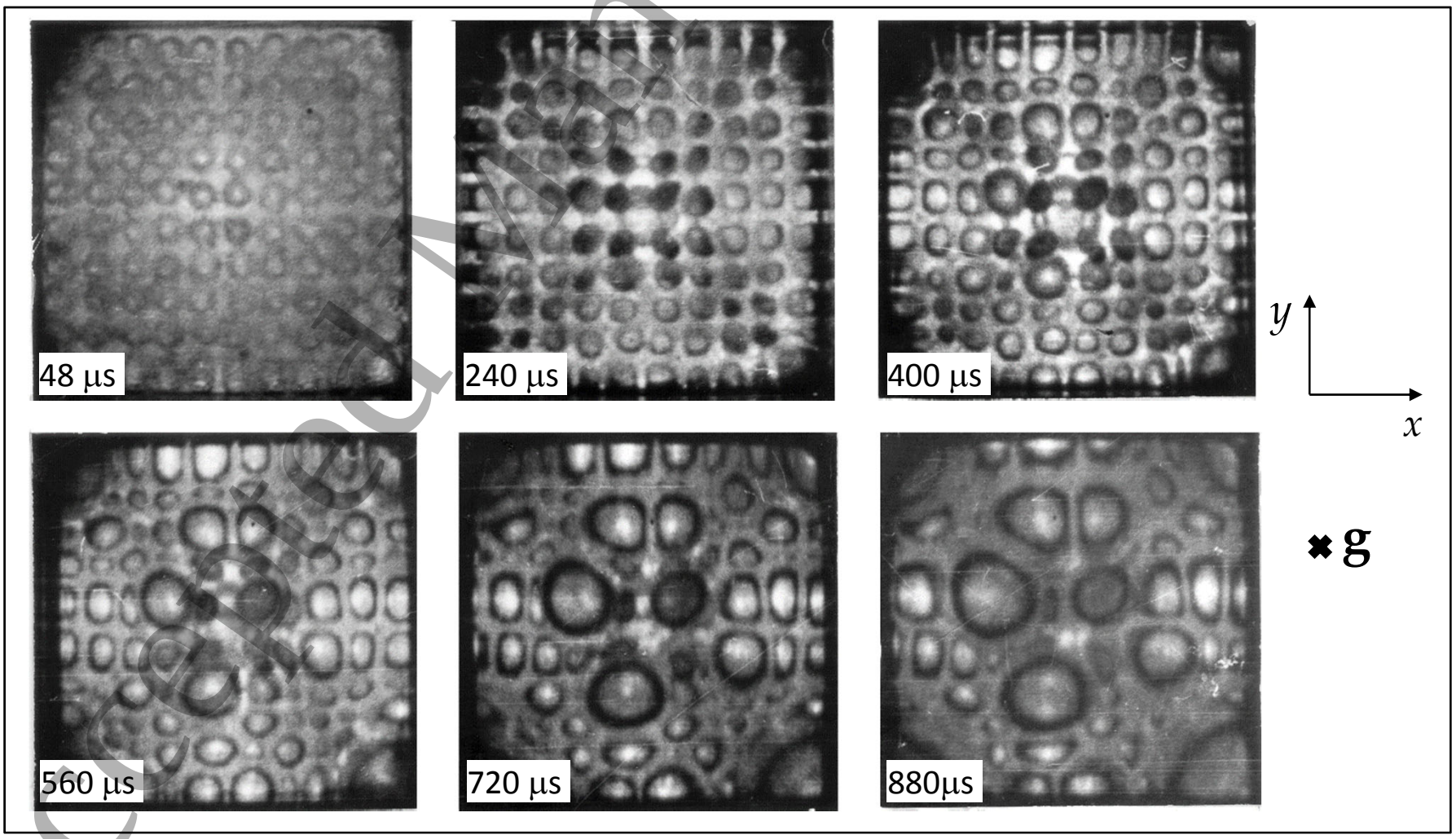

Figure 9

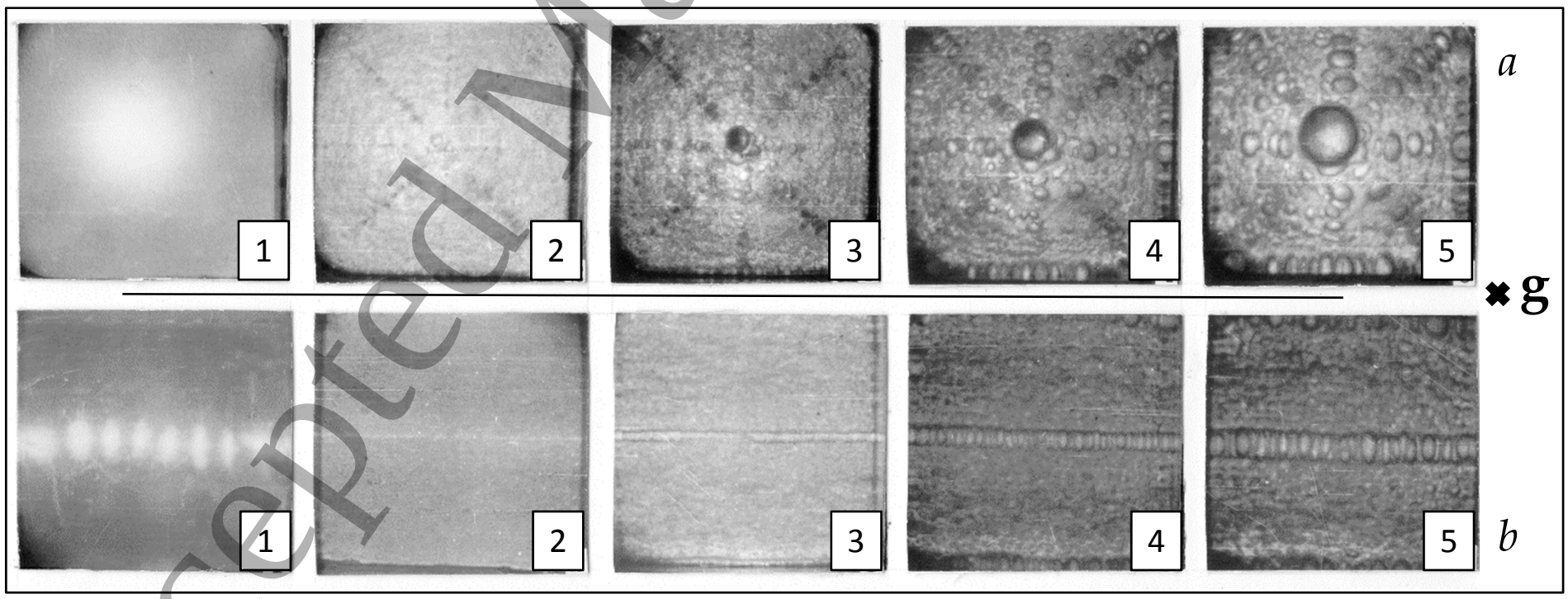

Figure 10

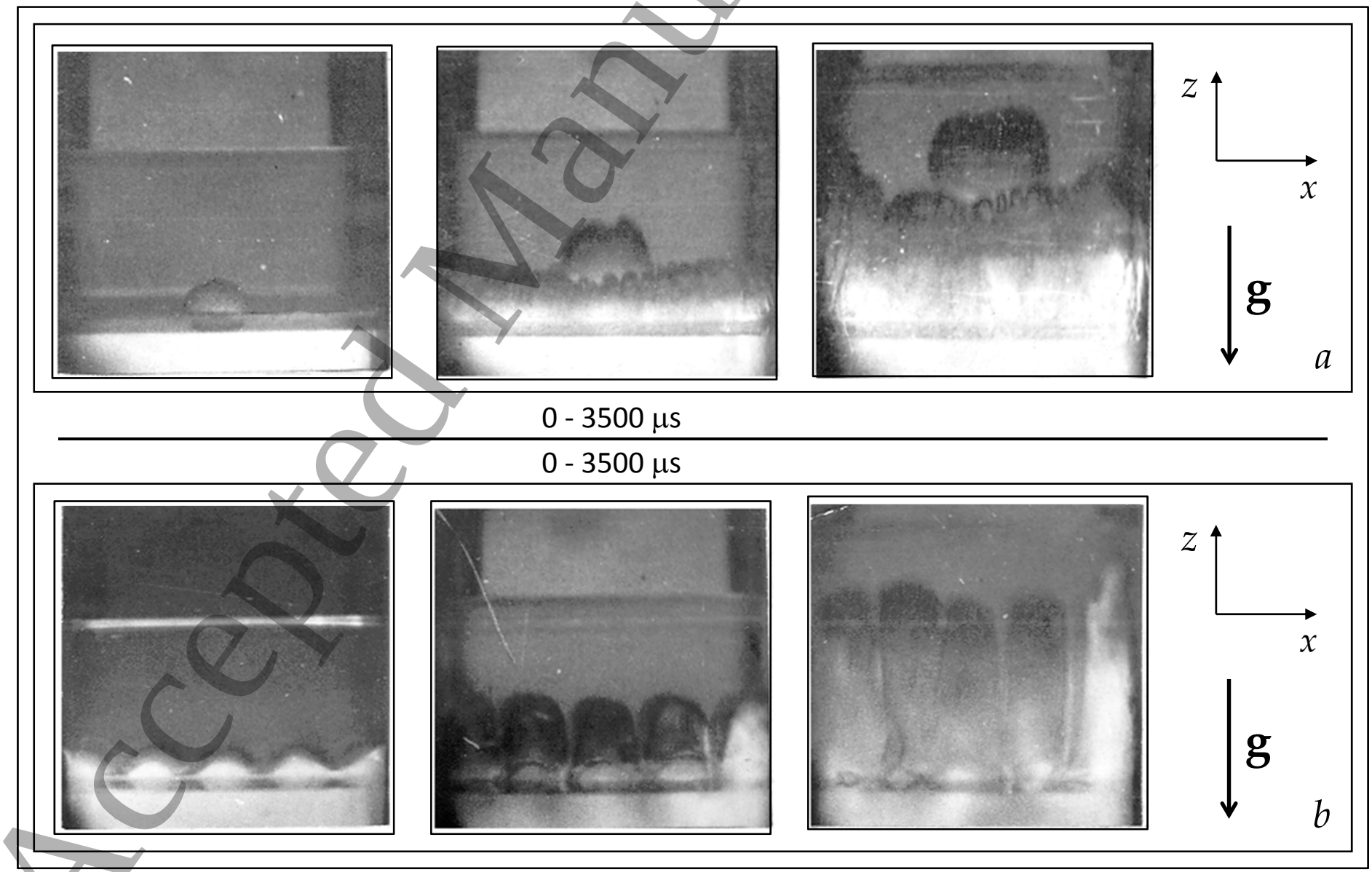

Figure 11

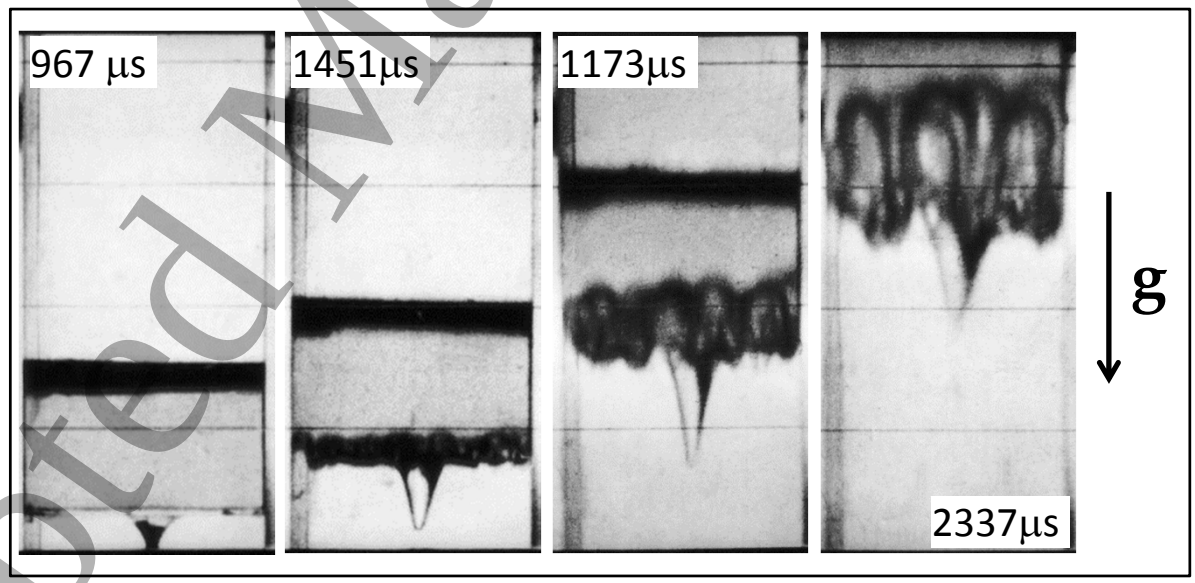

Figure 12

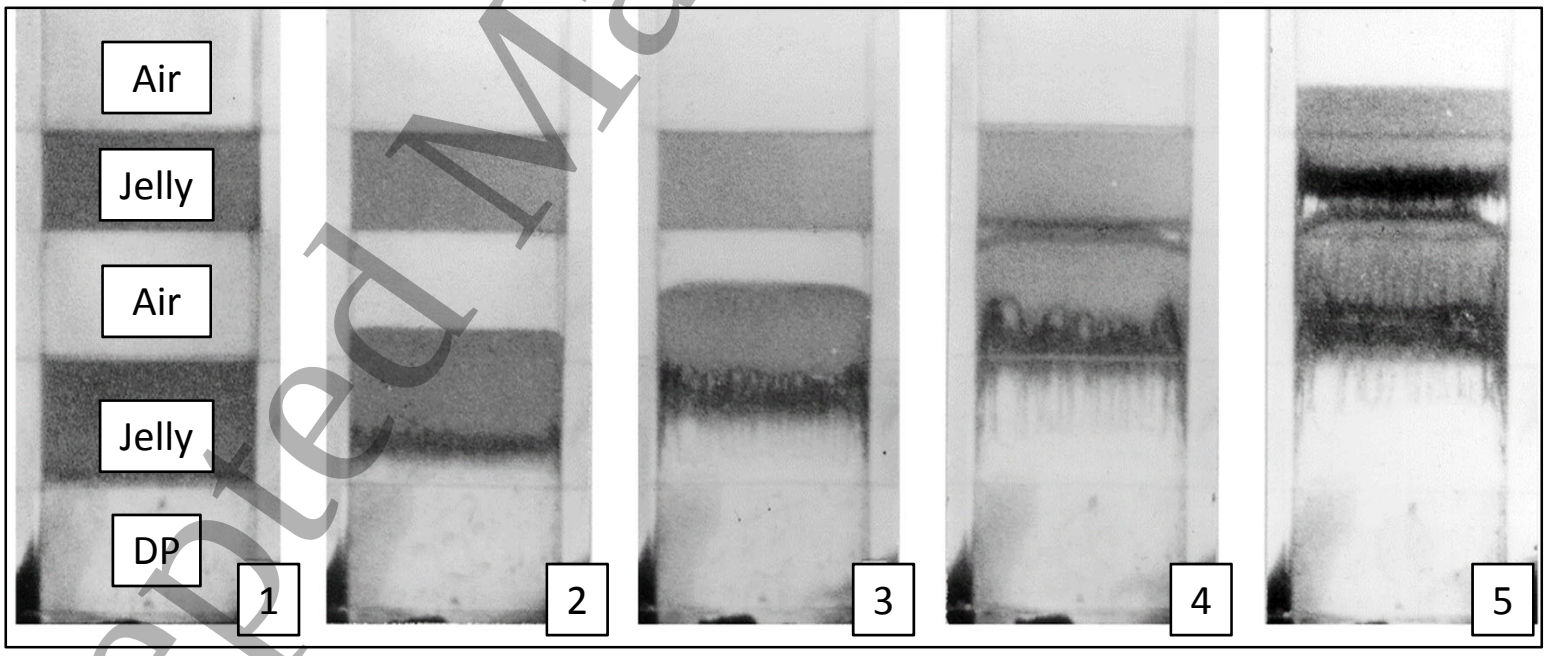

Figure 13

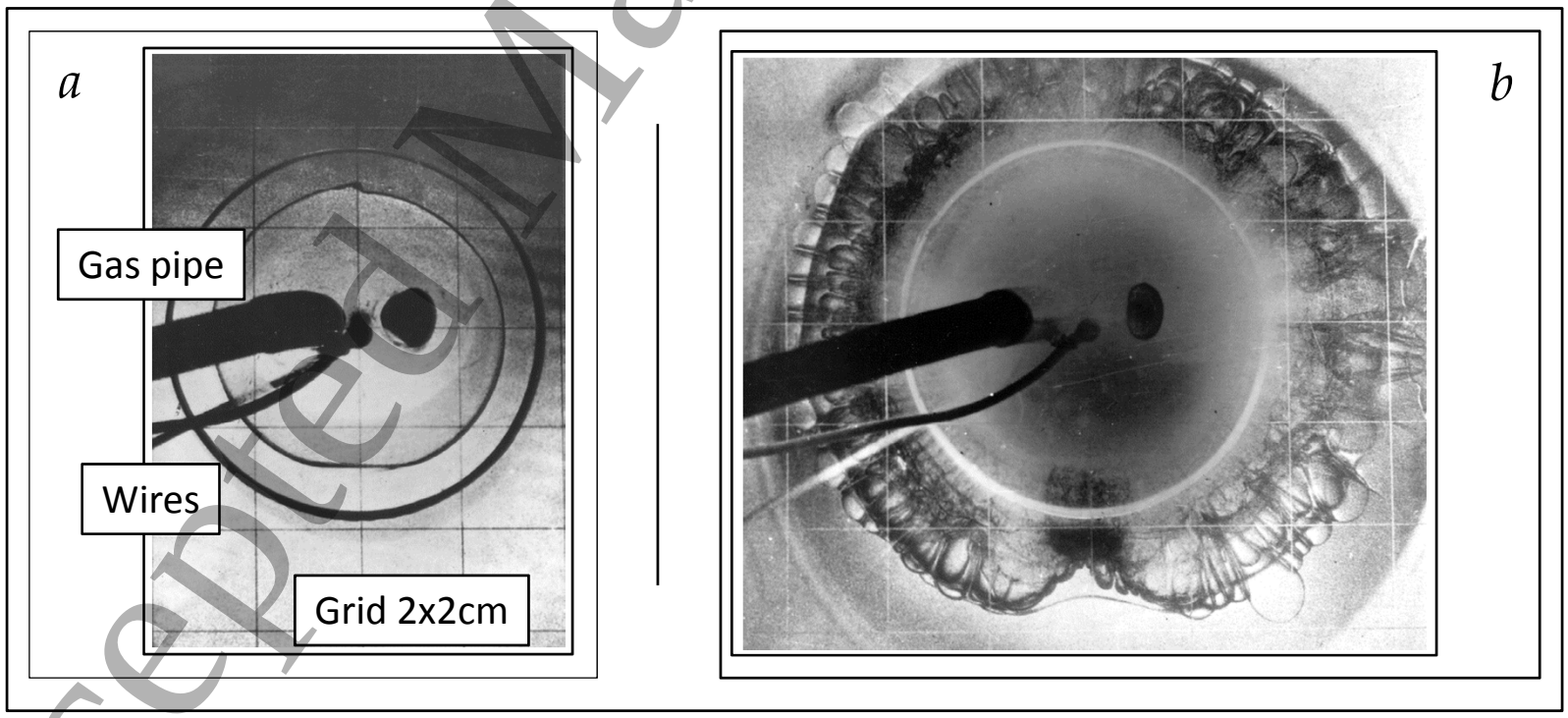

Figure 14

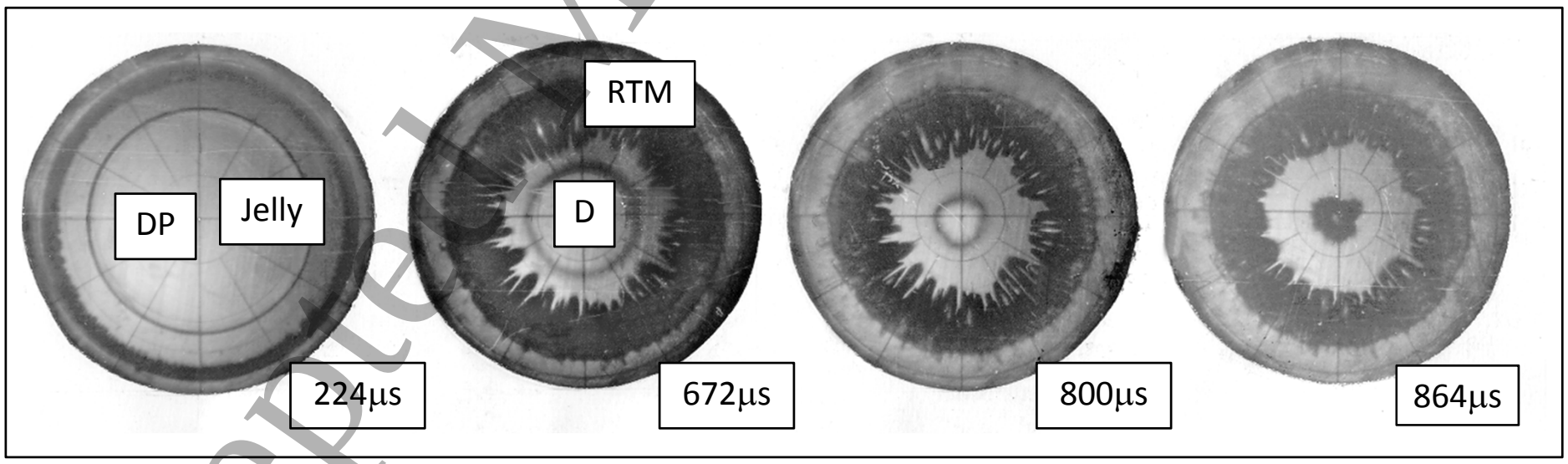

Figure 15